MICROWAVE MODULATION OF CO2 LASERS IN GaAs THIN FILM OPTICAL WAVEGUIDES

P. K. Cheo, et al

United Aircraft Research Laboratories

Prepared for:

Office of Naval Research
Advanced Research Projects Agency

29 March 1974

MICROWAVE MODULATION OF CO_2 LASERS IN GaAs THIN FILM OPTICAL WAVEGUIDES

SEMI-ANNUAL TECHNICAL REPORT

Period Covered: 25 September 1973 to 25 March 1974

Contract No. N00014-73-C-0087

Sponsored by

Advanced Research Projects Agency

ARPA Order No. 1860, Amendment No. 6

United Aircraft Research Laboratories

UNITED AIRCRAFT CORPORATION

EAST HARTFORD, CONNECTICUT 06108

64

N921513-6

Third Semi-Annual Technical Report

Microwave Modulation of CO_2 Lasers in GaAs Thin-Film Optical Waveguides

by

P. K. Cheo, M. Gilden, D. Fradin and R. Wagner
United Aircraft Research Laboratories
East Hartford, Connecticut 06108

March 29, 1974

Principal Investigator: P. K. Cheo (203) 565-4297

Prepared for the Office of Naval Research
Contracting Officer: Dr. M. White
Contract No. N00014-73-C-0087
Contractor Modification No. P00002 - $204,812.00
25 August 1972 to 25 June 1974

Sponsored by
Advanced Research Projects Agency
ARPA Order 1860, Amendment No. 9/11-15/72

N921513-6

Microwave Modulation of CO_2 Lasers in GaAs Thin Film Optical Waveguides

Table of Contents

1.0 Technical Report Summary

1.1 Program Objectives

The long-range objective of this program is to develop an efficient and reliable ultra-wideband thin-film modulator for CO_2 lasers that will be useful for high-resolution, imaging optical radars and high-data-rate optical communication systems. During the present reporting period (September 26, 1973 to March 25, 1974), the goal of this program is the demonstration of efficient sideband generation at microwave frequencies (X-band or Ku-band) from the 10.6 μm CO_2 molecular resonance. For the remaining contractual period (March 26, 1974 to June 25, 1974), the goal is to experimentally demonstrate the generation of frequency-chirped 10.6 μm CO_2 laser waveforms using the microwave-driven thin-film modulator developed under the present contract. Characteristics of the frequency chirped optical signals, sideband power limitations and total optical insertion loss of the microwave-driven thin-film modulator will be investigated. In particular, techniques for improving coupling efficiency of both optical and microwave power will be determined.

1.2 Method of Approach

In order to meet the goal of the present program, concentrated effort has been placed in four major areas of technology which require immediate attention. They are (1) the investigation of sideband generation and detection at a frequency 10 GHz offset from the 10.6 μm CO_2 laser carrier, (2) continuous improvement of fabrication techniques for thin-film optical waveguides, (3) theoretical study of efficient optical coupling and beam profiling by means of grating couplers, and (4) investigation of characteristics of a dielectric, thin-film-loaded, microwave mini-gap traveling structure at Ku-band.

1.3 Technical Program Plan and Schedule

The technical program consists of five basic tasks. They are:

Task 1: Microwave Modulation Experiment

This experiment is a very important step in the development of an ultra-wideband thin-film modulator. The success of this experiment sets the first milestone for the program. It demonstrates the practicality of our integrated optics approach for achieving efficient ultra-wideband modulation of CO_2 laser light. This task involves the generation of a sideband by using a microwave thin-film modulator developed under the present program and the detection of the sideband at a frequency 10 GHz offset from the CO_2 laser resonance by using an ir Fabry Perot interferometer. A detailed discussion of this experiment will be given in Section 2.0.

Task 2: Improved Techniques for Fabrication of Thin Film Waveguide Structures

This task involves the development of a new generation, thin-film optical waveguide for use in the microwave modulator. Investigations are being conducted to

evaluate a variety of high-resolution plates, positive and negative resists, and techniques for defect-free contact printing. Most important, an ion-milling machine will be adapted for use in the fabrication of gratings and finishing of GaAs thin-film surfaces. Detailed discussion on these techniques and some recent evaluations of gratings structures will be given in Section 3.0.

Task 3: Theoretical Investigation of Grating Coupling

This task involves a detailed calculation of coupling efficiency and optimum coupling length for specific grating structures fabricated in GaAs thin-film waveguides. Computer results have been obtained by using formulations derived from perturbation theory. A more rigorous approach utilizing the "leaky-wave" theory is also being used to describe grating coupling. Detailed analysis is given in Section 4.0.

Task 4: K$_a$-Band Microwave Structure

This task involves design, fabrication and evaluation of a wideband, mini-gap microwave traveling transmission line with a GaAs thin-film loading that operates in the frequency range from 12 to 18 GHz. Measurements of the characteristic impedance and losses in these frequency ranges were obtained. Detailed discussion on the microwave structure and measured results are given in Section 5.0.

Task 5: Frequency Chirping of CO_2 Lasers

This task involves an experiment study of the characteristics of a frequency-chirped CO_2 laser waveform generated by the thin-film microwave modulator that was developed under the present program. The experimental setup involves the use of two stable, line-selected CO_2 lasers, having a frequency difference of about 15.5 GHz. A sideband at 15.5 GHz offset from the molecular resonance of one of the two lasers is generated and will be modulated by using the thin-film microwave modulator. The frequency-chirped signal will be examined by means of a heterodyne receiver system which consists of a liquid-He-cooled Hg:Ge detector, a CO_2 (isotopic) local oscillator and a real time spectrum analyzer or a wideband oscilloscope. Detailed discussion of this task will be given in the next semiannual technical report.

The program schedule is presented in Table I.

1.4 Major Accomplishments

Various tasks are progressing in accordance with the schedule as shown in Table I. Three significant accomplishments have been realized during this interim reporting period. They are:

A. Sideband generation has been accomplished by means of microwave FM phase modulation of a CO_2 laser at X-band in a GaAs thin-film optical waveguide. The results of this work will be presented at the International Quantum Electronics Conference, June 10-13, 1974, in San Francisco, California.

B. Grating coupler analysis has been performed by both perturbation theory and leaky wave theory. Results of these calculations provide new guidelines for optimum design of optical waveguide structure.

C. Traveling microwave mini-gap ridge waveguide at Ku-band has been evaluated. Results indicate that a bandwidth > 2 GHz can easily be achieved and impedance matching can be accomplished simply by using one-step transformer network.

TABLE I – ARPA/ONR THIN FILM MODULATOR PROGRAM SCHEDULE

TASK	OCT	NOV	DEC	JAN	FEB	MAR	APR	MAY	JUNE
1.0 MICROWAVE MODULATION EXPERIMENT									
EXPERIMENTAL SETUP	———	———							
SIDEBAND DETECTION AND MEASUREMENT			———	———					
EVALUATION AND OPTIMIZATION				———	———				
2.0 IMPROVED FABRICATION TECHNIQUES									
HR PHOTOMASKS			———	———					
PHOTOLITHOGRAPHY AND SPUTTER–ETCH				———	———				
NEW CHEMO–MECH POLISHING PROCESS						———			
ION MILLING OF GaAs						———	———	———	
3.0 INVESTIGATION OF GRATING COUPLING									
PERTURBATION CALCULATIONS OF η					———	———			
PERT. CALC. OF OPTIMAL COUPLING α						———			
EXACT CALCULATION OF η AND α						———	———		
BEAM PROFILING CALCULATIONS							———		
NEW DESIGN ANALYSIS								———	———
4.0 Ku BAND MICROWAVE STRUCTURE									
DESIGN AND FABRICATION				———	———				
IMPEDANCE MATCHING NETWORK					———	———			
MEASUREMENTS OF PARASITICS						———	———		
5.0 FREQUENCY CHIRPING OF CO_2 LASER									
HETERODYNE DETECTION SYSTEM				———	———	———			
CONSTRUCTION OF MICROWAVE MODULATOR							———		
15.5 GHz SIDEBAND GENERATION								———	
MEASUREMENT OF FREQUENCY CHIRPING									———
REPORTS									
QUARTERLY MANAGEMENT			▲						▲
SEMI–ANNUAL TECHNICAL						▲			
PRESENTATION, O.E. CONFERENCE									▲

2.0 An Experiment for Sideband Generation and Detection at Microwave Frequencies

2.1 Introduction

Microwave modulation of ir laser beams for high-date-rate communication and optical imaging radar applications usually require very large amounts of driving power, P_d. The P_d values increase rapidly with increasing laser wavelength, λ. For conventional diffraction-limited bulk modulator crystals, an optimum value exists for the ratio of the modulator length to the cross-sectional area. By using optical waveguides, it is possible, in principle, to extend the modulator length substantially, and thus to reduce the driving power. For the case of thin film optical waveguide modulators, another advantage is that the voltage required to produce a charge of refractive index decreases linearly with decreasing the film thickness. At the 10 micron CO_2 laser wavelength, previous results[1,2] indicated that voltage applied to a GaAs thin film modulator can be reduced significantly. It is reasonable to expect that the modulation power can be made almost three orders of magnitude less than that required in bulk modulator crystals using identical electric field strength. However, a decrease in modulator thickness results in an increase in device capacitance or characteristic admittance which can severely limit the modulation bandwidth. This section describes a unique approach, by which ultra-wideband modulation of infrared laser radiation can be efficiently achieved by using a thin-film optical waveguide and a mini-gap microwave ridge waveguide. The modulation bandwidth limitation is minimized by choosing a microwave configuration which incorporates the device capacitance into a broadband microwave structure.

2.2 Integrated Optics Approach to Microwave Modulation of CO_2 Lasers

Electrooptic interaction in a nonlinear bulk single crystal between the 10 micron laser radiation, f_o, and a millimeter wave, f_μ, has been previously reported.[3,4] In this work, we report the observation of the sidebands at the sum and difference frequencies $f_o \pm f_\mu$, in a GaAs thin-film optical waveguide.[5] The interaction between optical guided-wave propagating in the [110] direction and a synchronous traveling microwave in [100] oriented thin-film produces a phase shift in the propagating mode. The purpose of this work is aimed at the generation of frequency-chirped optical signals at the sideband frequencies by using a frequency modulated microwave field.

Basically, the microwave thin-film electrooptic modulator is constructed by placing an optical ir waveguide inside a mini-gap microwave ridge waveguide. The GaAs thin-film optical waveguide that has a typical thickness of 20 microns is made by using a chemo-mechanical polishing technique. The optical coupling is accomplished by means of two phase gratings fabricated at the two ends of the GaAs thin-film by rf sputter-etch technique. The active length, L, of the modulator can be as long as 3.0 cm. Within this length, an intense traveling microwave field at either X-band or Ku-band is sustained in the thin-film underneath the narrow ridge region. Microwave measurements were made in structures as shown in Figure 1, where the width of the ridge is 0.1 cm. The measured values of the characteristic impedance and the attenuation coefficient in the range from 8 to 12 GHz through such a structure are shown

FIG. 1

PHOTOGRAPH OF RIDGE WAVEGUIDE TEST FIXTURE

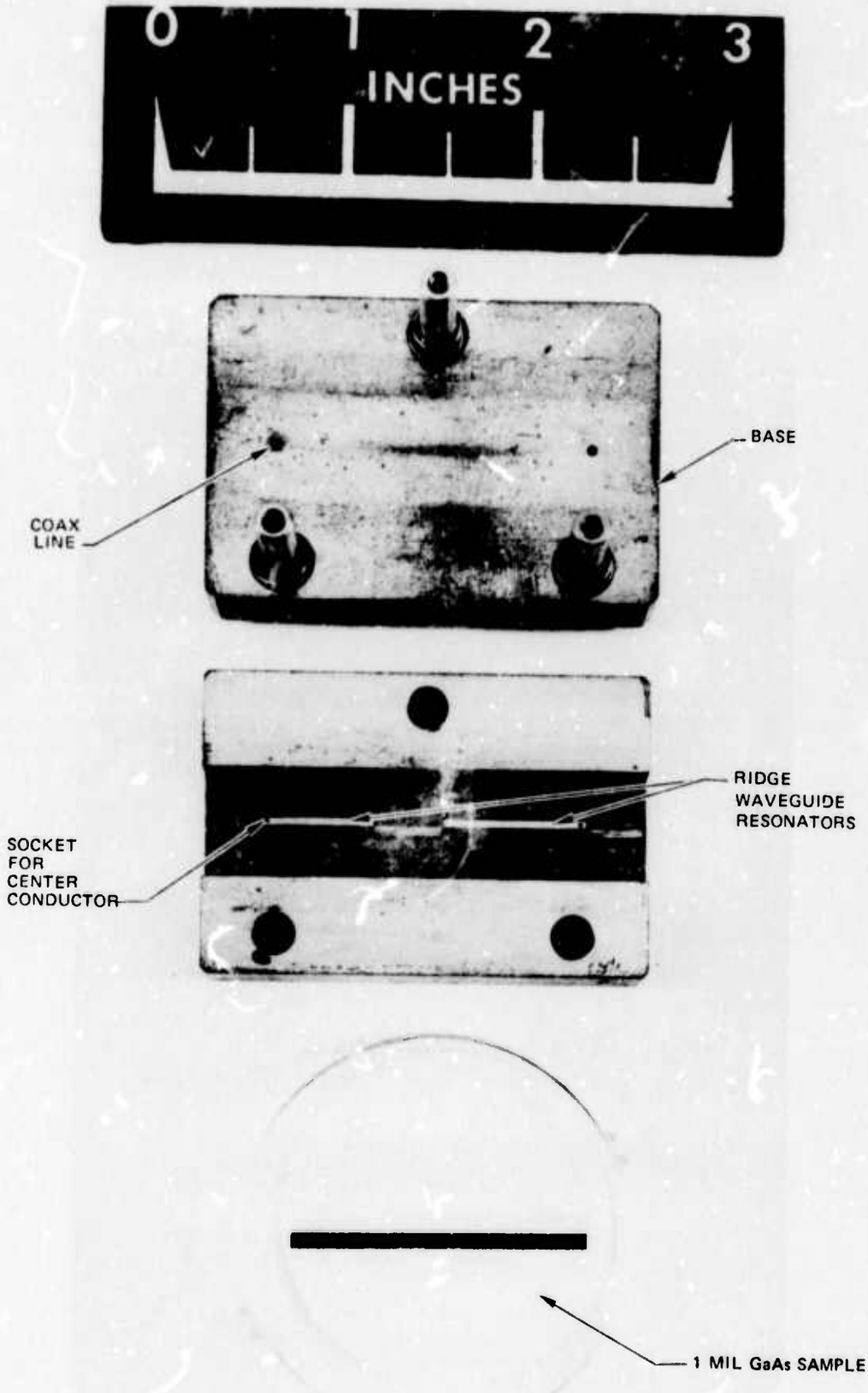

in Figure 2. These measurements are in agreement with our calculated values as presented in Section 5.

2.3 Experimental and Results

The experimental setup for the generation and detection of the sidebands at the sum and the difference frequencies, $f_o \pm f_\mu$, is shown in Figure 3. A single frequency CO_2 laser is collimated by means of front surface reflecting mirrors and then aligned with the input grating coupler of the thin-film modulator at a synchronous angle of incidence. The periodicity of the gratings ($\Lambda = 2.75\ \mu m$) is selected for phase-matching of a guided wave mode in the backward direction[6] through the back-surface of the thin-film. The output of the CO_2 laser radiation through the second grating coupler is optically aligned with a scanning Fabry-Perot ir interferometer, FPI. The FPI is adjusted so that in one free-spectral scan, its frequency will sweep over 24 GHz. The measured finesse is about 10 and corresponds to a half-width of 3 GHz, as shown in Figure 4. The upper trace is the ramp voltage wave-form which is adjusted for one free-spectral scan. The middle trace is the transmitted laser signal. The transmitted laser signal is focused by a f/1 Ge lens onto a liquid nitrogen cooled PbSnTe photo-diode. The detector signal after passing through a low-noise amplifier is displayed on the Tek 7904 oscilloscope. When 12 watts microwave power is applied to the thin-film modulator through a 1 cm long ridge section, both the upper and lower sidebands at $f_o \pm 10.2$ GHz have been detected, as indicated by the lower trace of Figure 4. These small sideband signals disappear when microwave field is removed from the thin-film. The estimated sideband power generated at 10 GHz is about 0.5 percent of the laser power.

It turns out that our approach represents an optimum solution for infrared lasers and microwave frequencies at X and Ku-bands because the dimensions of single mode optical waveguide for infrared lasers can be chosen such that broadband efficient microwave coupling can readily be obtained. A detailed study of the depth of modulation as a function of microwave power, the modulation bandwidth and linearity of frequency chirping is still in progress, and will be reported[7] later.

FIG. 2

MEASURED PARAMETERS OF NARROW GAP MICROWAVE MODULATORS

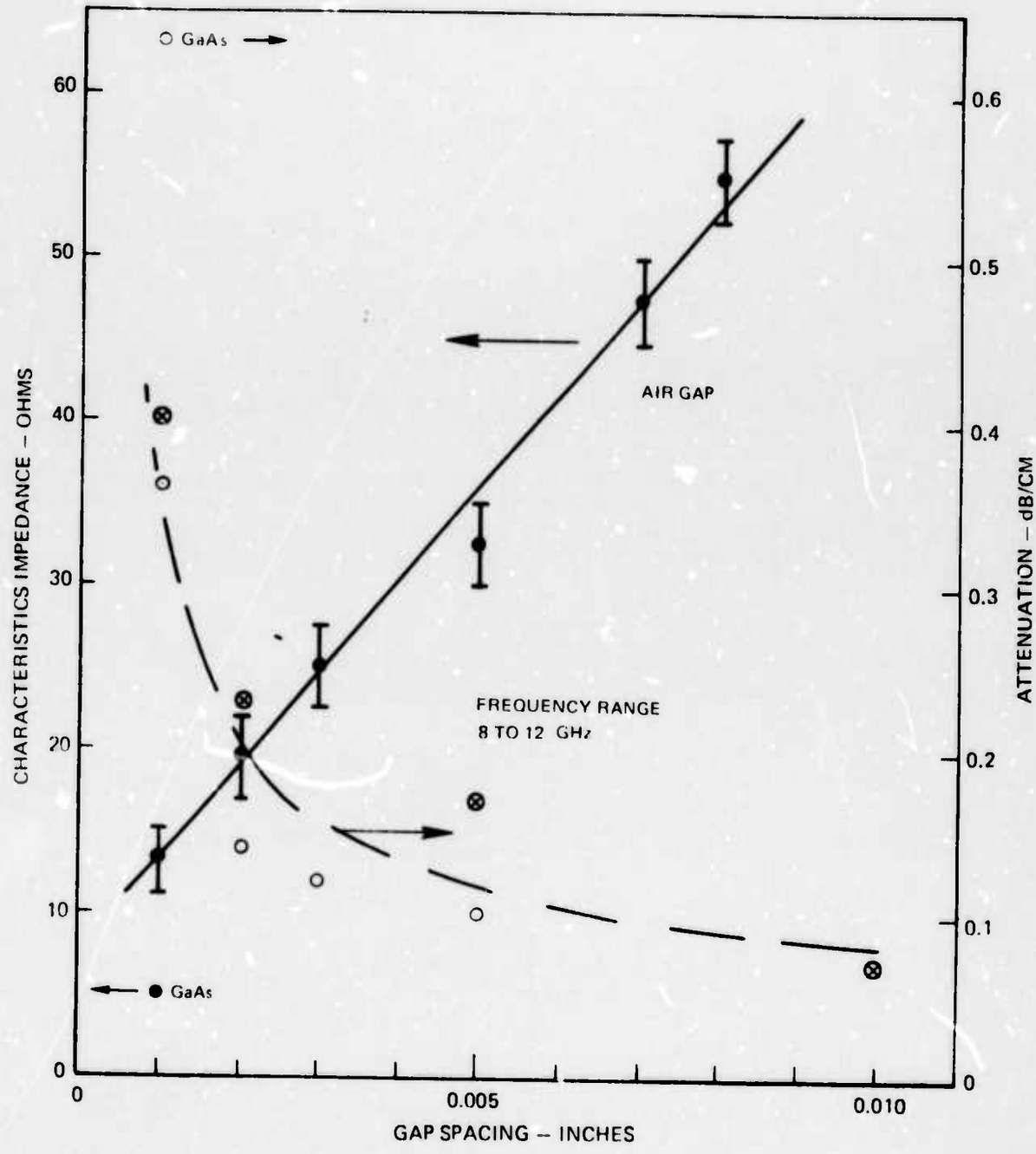

FIG. 3

BLOCK DIAGRAM OF MICROWAVE MODULATION EXPERIMENT

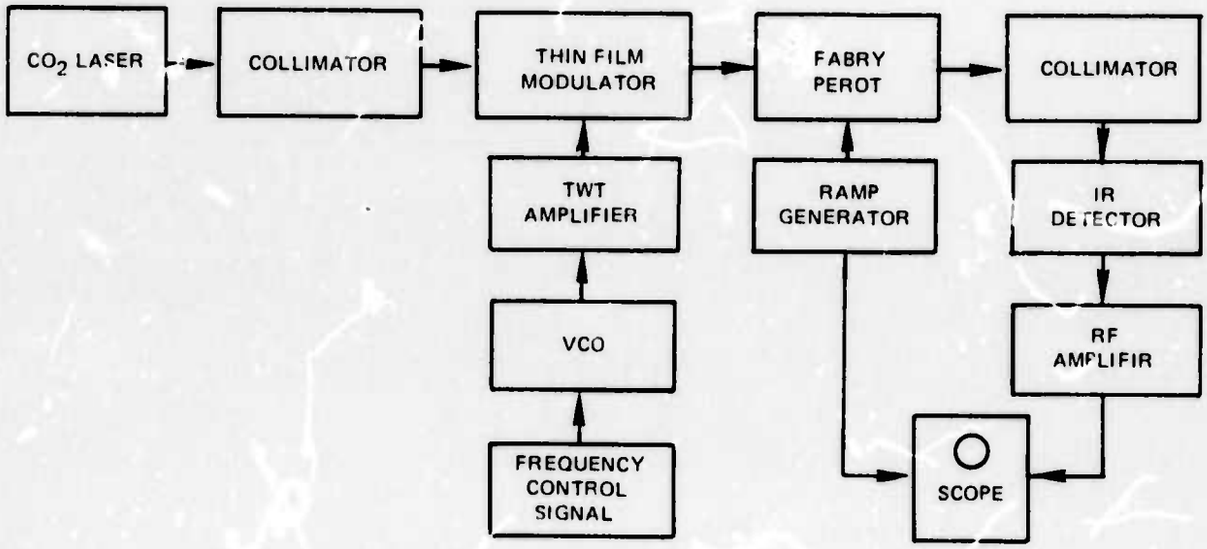

FIG. 4

SIDEBAND GENERATION AT MICROWAVE FREQUENCIES

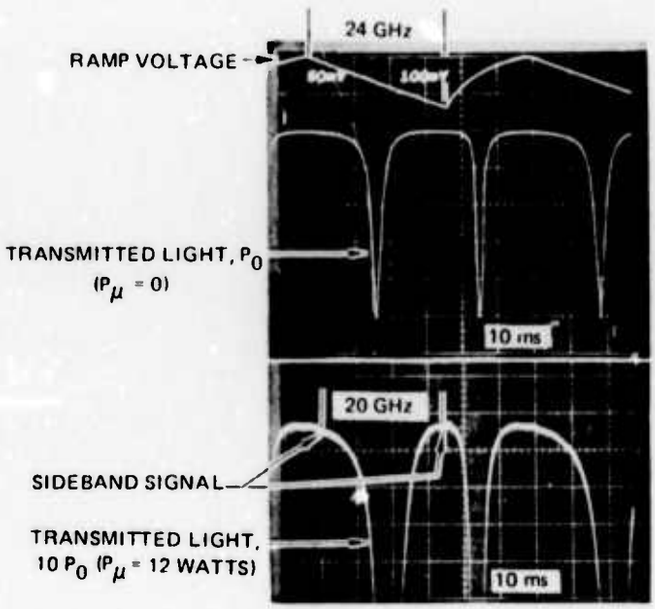

N01-126-1

3.0 Improved Fabrication Techniques for Optical Waveguides

3.1 Introduction

Thin-film optical waveguides used in this program are made by chemo-mechanical polishing of bulk wafers. This polishing technique has been described previously in detail[8] and provides mirror-like large surface (> 1 in^2) GaAs thin-films having thickness ranging from 20 to 40 μm. On the surface of these thin-films, two gratings are fabricated at two terminals separated by a distance ≈ 3 cm. These two gratings are important components of thin-film optical waveguides by which light must be coupled into and out of the thin-film efficiently and without distorting the beam shape. To accomplish this, one must first of all develop a technique for producing gratings reliably and repeatably from wafer to wafer so that accurate experimental data may be obtained.

This section describes techniques developed to improve fabrication of grating couplers. The processes involved in producing 2.75 micron periodicity diffraction gratings will be outlined. Some of the shortcomings of prior techniques will be pointed out, and methods for overcoming these drawbacks will be discussed.

3.2 Grating Fabrication Procedure

The method established was a refinement of previous techniques[14] implemented for grating fabrication. Briefly, the previous fabrication method utilized a chrome on glass plate as a master mask for imaging gratings on GaAs, which had been coated with films of SiO_2 and chrome. The chrome acted as an etch mask for the SiO_2 chemical etchant. The SiO_2 acted as a protective layer for that portion of GaAs not to be sputter etched.

Some of the drawbacks of the previous fabrication method must be realized before one can appreciate the present fabrication method. They are:

1. Processing of high resolution emulsion mask was marginal.
2. Producing a chrome on glass mask using the lift-off technique is not efficient.
3. Improper contact between chrome mask and wafer when imaging caused poor quality gratings.
4. The method of sputter etching resulted in poor quality gratings, and lacked repeatability.

The most crucial step in the overall fabrication procedure lies in the proper processing of photographic plates. These plates consist of a photo-sensitive emulsion on glass. The emulsion becomes soft during developing, and is prone to particulate matter attaching to the soft gel. Overflow rinsing techniques were established to minimize this problem. Improved drying techniques using methanol/

water solutions were incorporated to produce a more uniform mask. Temperature control of the developing bath was established to produce photo plates having consistent contrast.

Producing a chrome on glass plate using the lift-off technique has several inherent difficulties. The glass plate must be absolutely clean during the entire processing from photoresisting to developing if pinholing is to be avoided and proper chrome/glass adhesion is to be realized. Secondly, one must not allow the temperature during the sputtering process to become excessive. This will not only cause the photoresist to flow but also make its removal in solvents difficult. If pinholes are developed in the chrome layer after deposition, they could cause mask degradation over a period of time. To avoid the pitfalls of the lift-off technique as well as the pinholing of chrome, the working plates are now fabricated from an iron oxide on glass.

Iron oxide on glass plates have several attractive features. They are less susceptible to pinholing than chrome. They yield better edge definition in an etched image. They are opaque to ultraviolet, but transparent to visible light, an ideal situation for mask alignment on GaAs wafers.

Improper contact between chrome mask and wafer surface during imaging was corrected by designing a vacuum hold-down fixture specifically designed for GaAs wafers. This fixture takes the advantage of the slight flexibility of high resolution glass plates so as to force a more intimate contact between the wafer surface and the iron oxide mask.

Experiments with sputter etching has resulted in improved quality of sputter etched gratings. It was found that mounting the wafer on a quartz disc which, in turn, was mounted on a copper disc, and sputter etching in such a manner as to keep the wafer cool resulted in a more uniform grating.

The procedure for fabricating diffraction gratings on GaAs waveguides is given in Table II. With improved techniques at various stages of the processing cycle, we now obtain good quality gratings reliably and reproducibly from wafer to wafer. Figure 5 is a 1000X photograph of a 2.75 μm periodicity grating image on GaAs wafer. Photoresist used is Shipley 1350J. Thickness of this resist film is about 1 μm. As shown in Figure 5, the narrow lines are developed-out areas having a width approximately 0.9 μm. The image was obtained by an intimate contact printing using a Kodak high resolution glass plate.

Figure 6 shows a better quality grating imaged on a GaAs wafer by using an iron oxide on glass plate. Kodak 747 microresist is used in this case and the resist film thickness is about 1500 Å. It is obvious from Figure 6 that the edge definition of these grooves by using an iron oxide mask is considerably improved from the former one as shown in Figure 5. Figure 7 shows a 2.75 μm periodicity SiO_2 grating pattern on GaAs wafer. The ridges and grooves are made almost equal in width. This is a desirable feature for making a direct comparison between theory and experiment.

FIG. 5

A 2.75 MICRON PREIODICITY GRATING IMAGED ON A GaAs WAFER

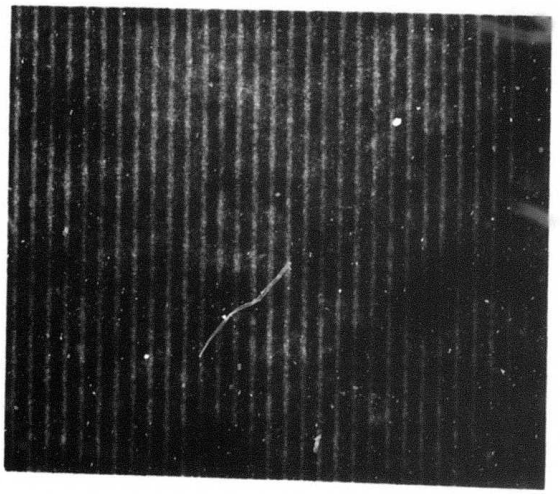

1000X

FIG. 6

AN IMPROVED 2.75 MICRON PERIODICITY GRATING IMAGED ON A GaAs WAFER

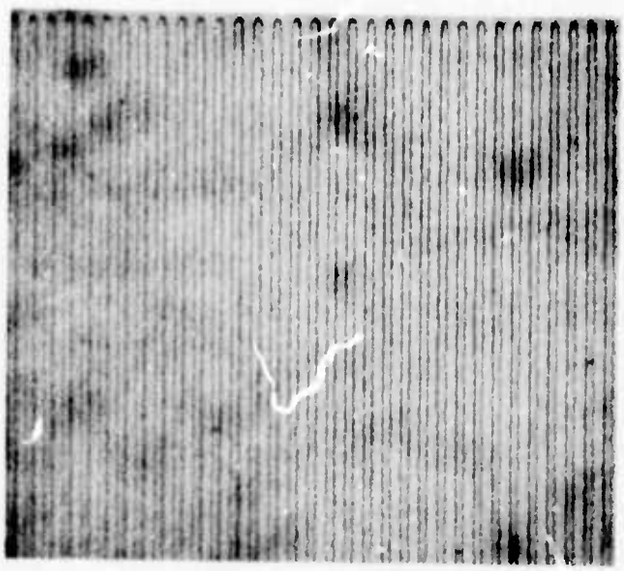

1000X

FIG. 7

A 2.75 MICRON PERIODICITY SiO_2 PATTERN ON A GaAs WAFER

1000X

TABLE II
A FLOW-CHART FOR FABRICATION OF THIN FILM WAVEGUIDE BY RF SPUTTERING

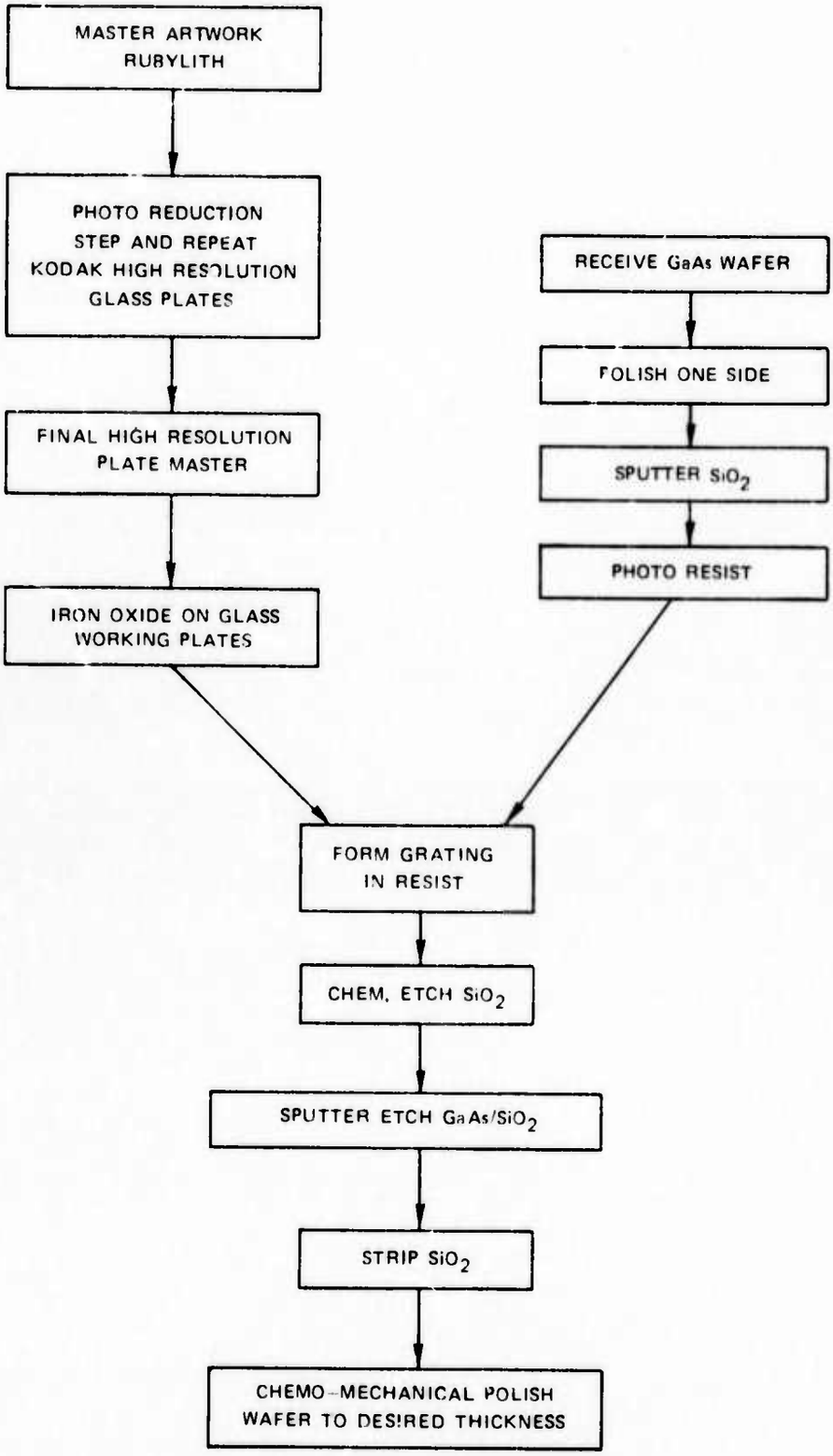

N03-268-1

3.3 Improved Techniques for Milling of Grating Grooves

At present, work is in progress to install an ion-milling facility. This facility will soon be used for fabrication of optical grating to replace the rf sputter-etch machine. Figure 8 shows the ion gun head purchased from Thomson CSF in France. The addition of this operation will further increase our ability to produce uniform grating grooves with edge definition as good as the mask shown in Figure 7. The major advantage of using ion-milling machine is that the substrate being etched is out of the plasma region where pressure is low. A collimated neutral beam will sputter GaAs material through the mask without raising the temperature of the substrate. It is possible to produce grating patterns with a thin layer of photoresist only.

Differential etch rates, as reported by the ion mill manufacturer - Veeco Instrument Company, are:

$$\frac{\text{GaAs}}{\text{SHIPLEY RESISTS}} = \frac{4}{1}$$

$$\frac{\text{GaAs}}{\text{KODAK RESIST}} = \frac{6.5}{1}$$

Techniques have been developed so that 2.75 μm periodicity gratings can be imaged in resist coatings having a thickness approximately one micron. With the ion mill and the improved photolithographic techniques, our fabrication process can now be reduced to the steps as shown in Table III.

TABLE III
PROCEDURE FOR FABRICATION OF THIN FILM WAVEGUIDE BY ION MILLING

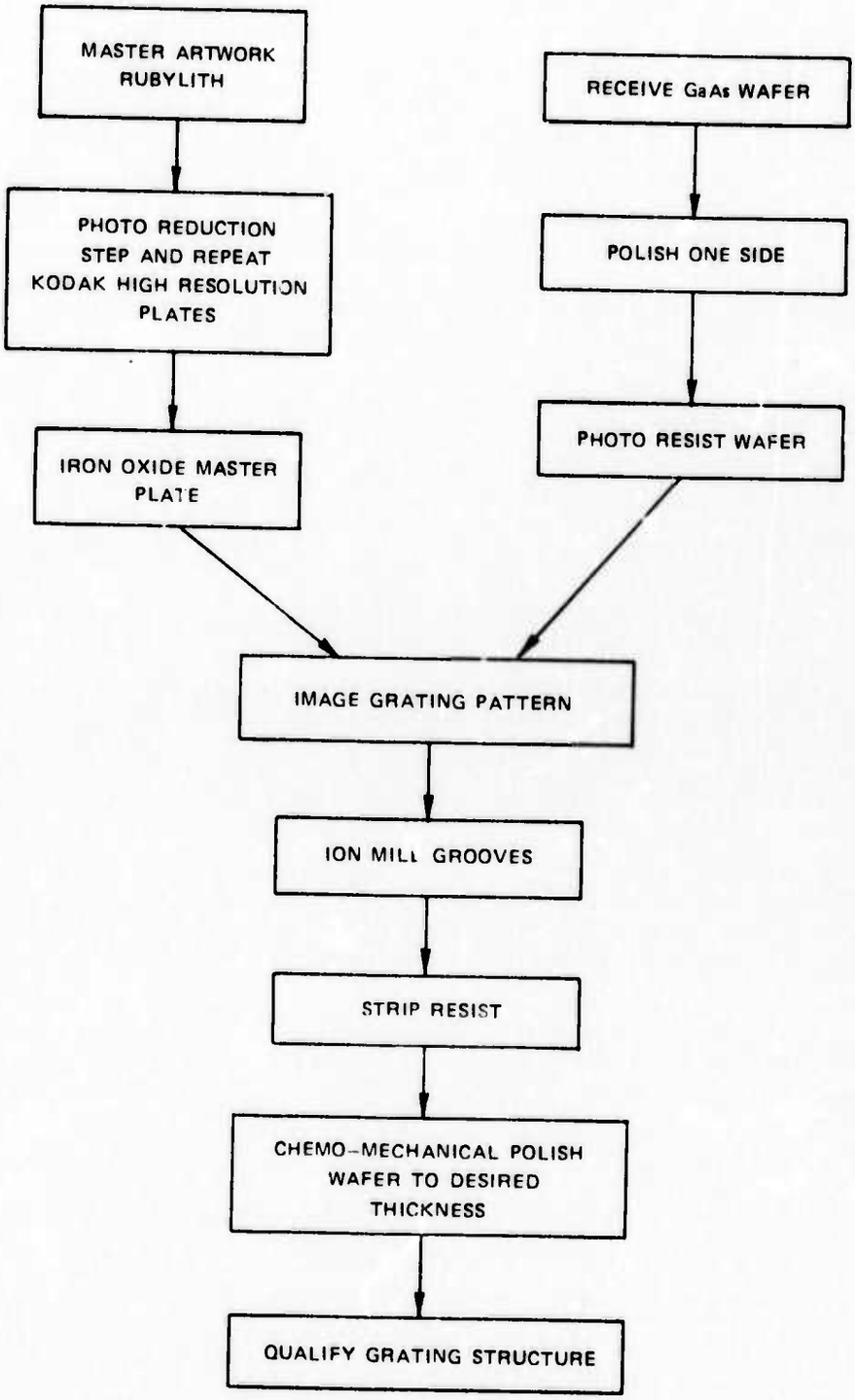

FIG. 8

ION BEAM MILLING MACHINE HEAD

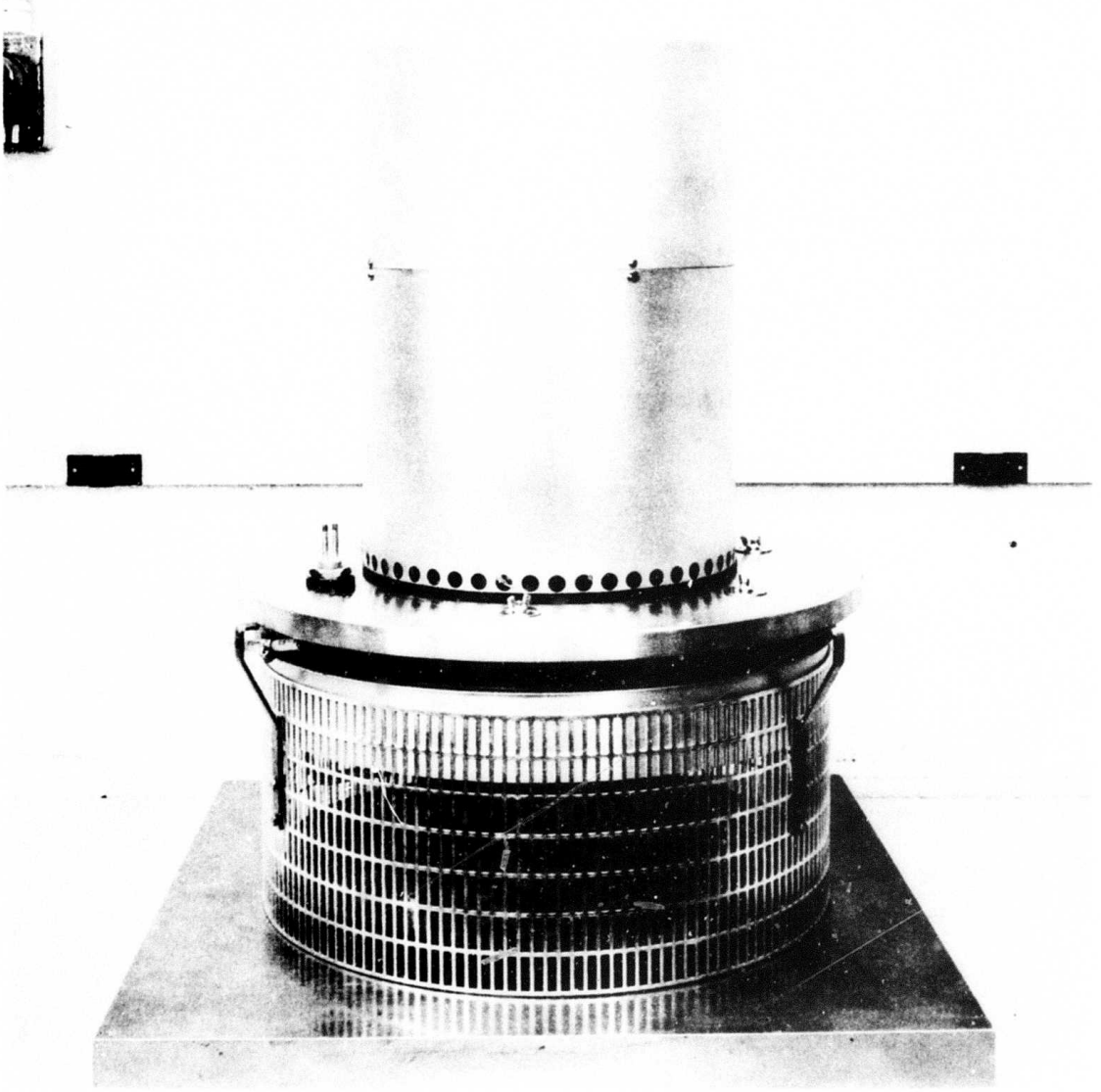

4.0 Design Analysis of Efficient and Profiled Grating Couplers

4.1 Introduction

Input-output couplers are of fundamental importance to the development of optical waveguide devices. The first significant advance in the field of integrated optics was the development of the concept of evanescent wave coupling. This concept led to the first significant air-film coupling experiment[9] conducted with a prism coupler. Coupling was accomplished by controlling the overlap of the exponential tail of the guided-wave and the evanescent field of the prism in the air-gap. This concept can be extended to treat the grating coupling problem. Mathematical formalism can be derived from a number of approaches, e.g., (1) coupled mode theory,[10] (2) perturbation theory,[6] and (3) leaky wave theory.[11] In this section, we shall first consider the loss mechanism of a grating coupler, which can be described by a parameter α, known as the attenuation constant. A discussion of the physical meaning of α and its implications for input and output coupling efficiency η is presented. This discussion is followed by a detailed calculation of values of α and η by the perturbation treatment. Finally, a brief discussion of techniques for tailoring the output beam shape is given.

4.2 Loss Mechanism of Grating Couplers - A Leaky Wave Approach

Optical coupling between a guided and an air mode can occur only when the two modes are phase-matched. Although the phase-matched condition cannot be established in a nonperiodic structure, the presence of a periodic structure introduces Fourier components to the guided wave that can phase-match to the air mode. The phase-matched condition for the Fourier component of the perturbed surface wave leads directly to the grating equation, as given by

$$\beta_m - k \sin \theta = 2\pi m/\Lambda \qquad (1)$$

where β and k are propagation constants of the guided and the air modes, respectively. Λ is the grating period, and θ is the coupling angle measured from the normal to the grating plane. There are two situations; namely

$$\theta > 0 \quad \text{(forward coupling)}$$
$$\theta < 0 \quad \text{(backward coupling)} .$$

As discussed in the previous technical report,[8] backward coupling is preferred for thin-film devices. The reason for this preference is that by using backward coupling, it is possible to eliminate diffraction into all grating orders m such that $m > 1$. Since diffraction into these higher orders represents an unwanted energy loss, the fraction of incident optical power coupled into the guided mode is maximized by the use of backward coupling.

A guided wave propagating in x direction can be written as

$$E(x,y,z,t) = E_s(y,z) \exp i(\omega t - \beta x). \qquad (2)$$

If losses exist because of scattering from closely spaced inhomogeneities, absorption, or diffraction into radiating modes, then β becomes complex and the mode is no longer a true surface mode. When β is complex, the mode becomes a leaky wave.

Leaky waves have been studied at microwave and optical frequencies.[11,12,13] The optical problem that most concerns us is, of course, the coupling between optical surface modes and radiation modes with the coupling created by a periodic structure. For convenience, we will initially consider only an output coupler and consider only a single diffracted beam. The basic generalization to many diffracted beams will then be simple. Of particular importance in the present discussion will be the physical meaning of the attenuation constant α, the form factor or coupling efficiency η, and the intensity distribution of the out-coupled beam.

In the presence of the grating, the propagation constant of the leaky waveguide mode becomes $\beta + i\alpha$, where β and α are real quantities assumed to be independent of propagation coordinate x. As a result, the amplitude of the leaky wave then decays as $\exp(-\alpha x)$ for $x > 0$. The functional form is a meaningful description of the leaky wave only in the limit where the radiation loss over a period d is small; i.e., when $\alpha\Lambda << 1$. Calculations of α[6,11] indicate that this condition is easily met for all grating configurations of practical interest.

Since the energy lost by the leaky mode must be gained by the radiating air mode, the air mode must have the same exponential shape in the near field just above the grating as the leaky wave. Its amplitude can be calculated from the requirement that for an infinite grating the energy of the guided mode incident on the grating at $x = 0$ must be equal to the integrated energy in the air mode. Assuming for simplicity that the two light waves are large and uniform in the y-direction, the energy balance becomes:

$$W_G = b \int_0^\infty [E_a(x)]^2 dx \tag{3}$$

where W_G is the initial energy in the guided mode; b represents appropriate constants; and the electric field of the air mode is given by:

$$E_a(x) = E_A \exp(-\alpha x). \tag{4}$$

Using Equation 4 to evaluate Equation 3 gives:

$$E_a(x) = \left(\frac{2W_G}{b}\right)^{1/2} \alpha^{1/2} \exp(-\alpha x)$$

$$\sim \alpha^{1/2} \exp(-\alpha x) \tag{5}$$

When α is a function of propagation distance, Equation 5 must be generalized to:

$$E_a(x) \sim \alpha(x)^{1/2} \exp\left[-\int_0^x \alpha(x)dx\right]. \tag{6}$$

Equation 6 summarizes the shape of the radiated air mode in the near field adjacent to the grating. As the mode propagates, its field distribution changes as shown schematically in Figure 9 for the case of constant α. Calculations of the Fresnel and Fraunhofer distributions of $E_a(x)$ for constant α have been made by Tamir.[14,15] In the discussion that follows, we will only be concerned with the region directly above the grating where Equation 6 is valid.

Having considered the amplitude variations of the leaky wave and the radiated beam, we now consider their phase variation as described by the propagation constant β'. Because $\alpha\Lambda \ll 1$, the grating only mildly perturbs the surface mode over a distance equal to the grating period d where d is of order λ/n_f and n_f is the waveguide's index of refraction. It is to be expected, therefore, that the phase perturbation over a distance d - i.e., $(\beta - \beta')\Lambda$ - is also small so that $\Delta \equiv (\beta - \beta')/\beta \ll 1$. The fact is illustrated with a perturbation calculation as we now show.

Consider a grating in which rectangular grooves with unit aspect ratio and depth δ are etched into a film of thickness t. It is well known that for a particular mode the propagation constant depends on the waveguide thickness. Outside the grating region $\beta = \beta(t)$ whereas inside the grating region $\beta' \approx \beta(t_{eff})$. The effective film thickness t_{eff} is approximately $\delta/2$ so that for small δ

$$\Delta = \frac{1}{\beta(t)}\left[\beta(t) - \beta(\delta/2)\right] \approx \frac{1}{\beta/k}\frac{d(\beta/k)}{dt}(\delta/2) \qquad (7)$$

As will be discussed in the next section $(\delta/2)/t < 0.1$ for gratings of practical interest so that Equation 7 is normally an accurate approximation. Tien[16] has evaluated $d\beta/dt$ for a thin-film guide. His results can be cast in the form:

$$\frac{1}{\beta/k}\frac{d(\beta/k)}{dt} = \frac{n_f^2 - (\beta/k)^2}{(\beta/k)^2}\left(\frac{1}{t'}\right)$$

where $t' = t + 1/p + 1/q$, and p and q describe the evanescent tails in the air and the substrate, respectively. For the symmetric multimode waveguides used in our thin-film modulator, $t' \approx t = 25\ \mu$, $n_f = 3.275$, and $\beta/k = 3.141$ for the TE_1 mode. Therefore:

$$\Delta \approx 0.0533\frac{\delta/2}{t}$$

Since $(\delta/2)/t \approx 0.1$, $\Delta \approx 0.005$. This value is considerably less than the mode separation in the GaAs waveguide. An upper bound to Δ under these conditions can be shown to correspond to $\beta/k \approx$ and $t' \approx 3t$ so that $\Delta_{max} \approx 0.3$, a value appropriate to high-order surface waves very close to cut-off.

On the basis of this calculation, we see that, as expected, the real part of the propagation vector is virtually unchanged by the presence of gratings of practical interest. This fact is important because it indicates that the guided surface wave can enter and leave the grating region with negligible reflection

FIG. 9

VARIATION OF $E_a(x)$ WITH PROPAGATION IN THE z DIRECTION (PERPENDICULAR TO THE WAVEGUIDE PLANE)

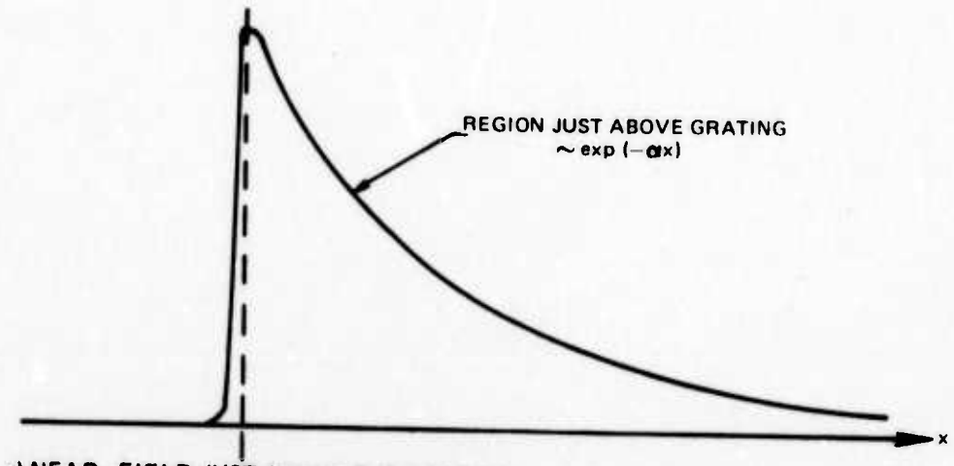

a) NEAR–FIELD JUST ABOVE THE GRATING

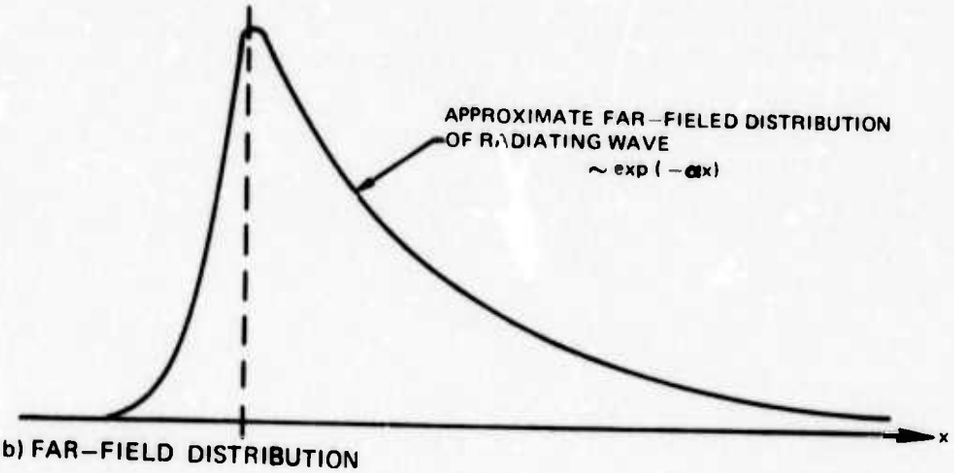

b) FAR–FIELD DISTRIBUTION

losses at x = 0. To a good approximation, then, the grating merely transforms the propagation vector from a real value β to a complex value $\beta + i\alpha$ with Equation 6 being a consequence of $\alpha \neq 0$. It can be shown that a prism coupler has these same properties.[16]

The discussion thus far has considered the phase and amplitude of both the leaky and radiated waves where the latter applies principally to a grating used as an output coupler. A direct consequence of the amplitude distribution Equation 6 is a form factor that describes the total diffraction efficiency of either a grating or a prism coupler when the coupler is used to couple energy into a guide. This form factor provides a simple and powerful analytical result that is useful in the design and understanding of grating input couplers.

The form factor is derived from an optical reciprocity argument.[16] For an infinite grating characterized by $\alpha(x)$, all the guided light is coupled into the radiating air mode that has an amplitude distribution $E_a(x)$ given by Equation 6. If the same grating is used as an input coupler, all the incident laser light can be coupled into the waveguide if the input beam $E_{in}(x)$ has the field distribution $E_a(x)$ and, of course, travels in the direction exactly opposite to $E_a(x)$. In general, $E_{in}(x) \neq E_a(x)$ so that some of the light is reflected. The fraction η of light that is coupled into the waveguide is related to that portion of the incident field that matches $E_a(x)$. In particular,[16]

$$\eta = \frac{\left[\int_0^\infty E_{in}(x)\, E_a^*(x)\, dx\right]^2}{\int_0^\infty E_{in}E_{in}^* dx \int_0^\infty E_a E_a^* dx} \qquad (8)$$

where the numerator is an overlap integral (or generalized vector projection along a basis function). If α is a constant and $E_{in}(x)$ is a beam that is uniform from x = 0 to x = 2R then Equation 8 simplifies to the form factor:

$$F = \frac{1}{\alpha R}\left(1 - e^{-2\alpha R}\right)^2 . \qquad (9)$$

Equation 9 is plotted in Figure 10 where it is seen that F has a broad maximum with a peak value of 81 percent when $\alpha R = 0.625$. It should be emphasized that R is the projected radius of the input beam with $R\cos\theta$ being the actual beam radius.

Equation 8 can also be evaluated for a Gaussian beam that varies along the x direction as $\exp(-x^2/w^2)$. The resulting integral in the numerator is a complimentary error function with a peak value of about 80 percent when $w\alpha = 0.68$. As before, the actual beam radius is $w\cos\theta$. The plotted shape of η for a Gaussian is very similar to Figure 10.

Although we have only considered a single diffracted beam in the present discussion, the results are directly applicable to multi-beam grating problems. Each radiating diffracted beam from a grating output coupler has the form of Equation 6.

FIG. 10

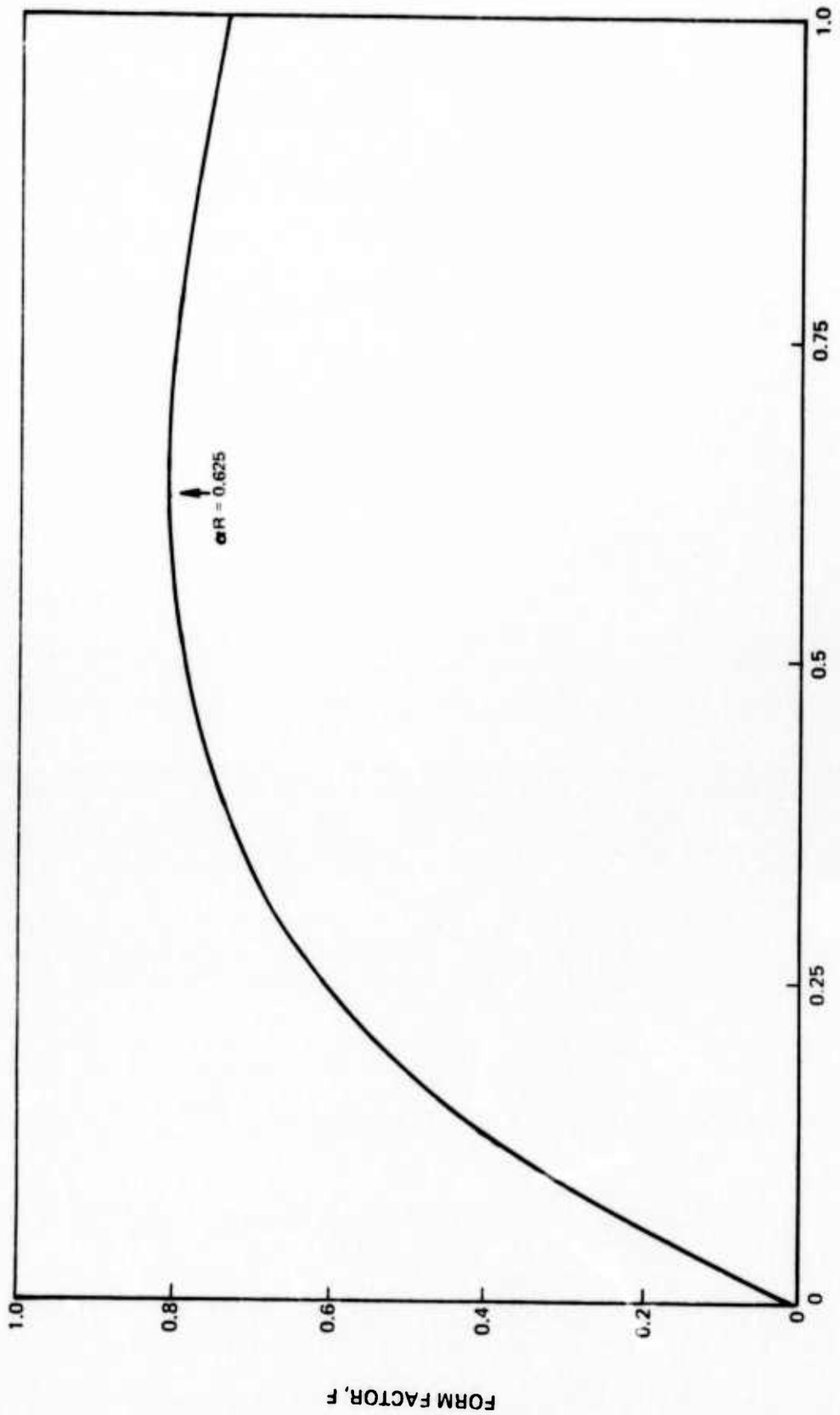

N03–225–1

Since reciprocity is, of course, valid for multiple beams, Equations 8 and 9 still measure the fraction of input energy coupled into diffracted beams although this coupled energy is now shared among the leaky wave in the waveguide and all other diffracted beams. The present results give no information on the fraction of light that is actually coupled into the leaky wave when more than one diffracted beam exists. The fraction of energy $(1 - \eta)$ that is not diffracted is lost by reflection at the grating plane. Figure 11 illustrates these ideas for a grating pair in a symmetric waveguide.

The laser power incident on the waveguide in Figure 11 is one watt; the Gaussian beam size is assumed to satisfy $\alpha w = 0.68$ so that $\eta(\max) = 80$ percent; and it has been assumed that the waveguide thickness and grating geometry have been adjusted so as to equalize the distribution of the energy into the two diffracted beams. It is seen that even when the grating coupling efficiency is at its maximum value (for a uniform grating) and only one diffraction order ($m = 1$) is possible, the existence of an extra diffracted beam can reduce the total energy transmitted through a grating pair by about an order of magnitude. If $\alpha w \neq 0.68$, more energy will be lost by reflection and, therefore, less energy will be available for the diffracted beams. Also, if the output grating is not sufficiently long to couple virtually all the guided energy into radiated modes, then the total useful output energy will be further reduced.

Placing an antireflection coating along the bottom of the waveguide will change α. If the beam size is adjusted to maintain the same value of αw, however, η will not change and the AR coating will have no effect on the grating performance. Unlike the use of AR coatings, blazing the grating (i.e., altering the groove geometry) can have a beneficial effect on the performance of the waveguide in Figure 11, because blazing will alter the distribution of energy into the diffracted orders. If αw is held constant, however, blazing will not affect the total diffracted energy. A quantitative prediction of the diffracted energy distribution for a blazed grating requires detailed calculations that properly account for the grating thickness and the exact blazing geometry. When only a single diffracted beam is allowed and w can be adjusted to maintain a constant value of αw, blazing also has no effect on grating performance.

To summarize: The phase grating coupler has been shown to transform a guided mode with real propagation constant β into a leaky mode with complex propagation constant $\beta + i\alpha$ where α is real and positive. By using the calculated amplitude distribution of the air mode radiated from an output coupler and requiring optical reciprocity, we have determined the coupling efficiency of an input grating. This coupling efficiency (or form factor) is equal to the total fraction of energy diffracted into all beams that satisfy the phase matching condition. Its values gives no information on the distribution of energy among these various diffracted beams. If the grating/waveguide system is designed such that only a single diffracted beam is allowed, the results of this section and the last section, completely describe the operation of grating couplers in terms of α and β where α is determined by the characteristics of the coupling regions and the allowed values of β can be found by usual waveguide analysis.[5]

DISTRIBUTION OF ENERGY IN A THIN FILM WAVEGUIDE FOR OPTIMUM COUPLING

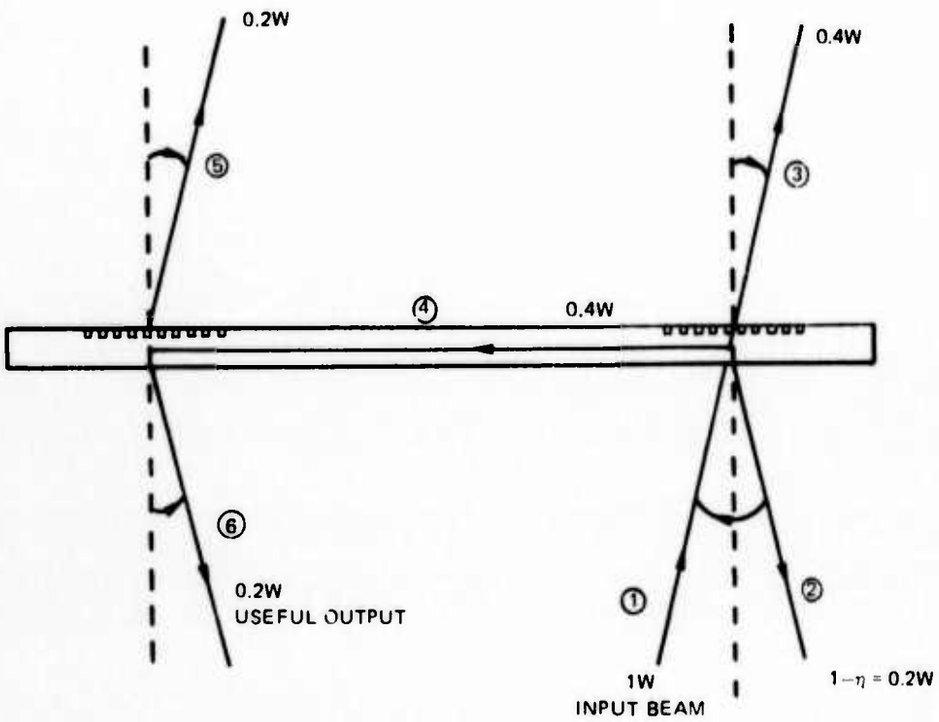

The total fraction of incident energy in ③ and ④ is η and cannot exceed ~ 80% for a uniform grating. The ratio of energy in ③ to energy in④ is the same as the energy ratio of ⑥ to ⑤. It's value depends in a complicated manner on the grating and waveguide geometries. A value of unity is assumed for convenience. The output grating is assumed to be sufficiently long to couple out all the guided energy.

4.3 Calculations of Efficiency and Optimum Coupling Length - Perturbation Theory

The value of the attenuation constant α depends in a complicated manner on the grating geometry, the waveguide thickness, and the indices of refraction of the waveguide and surrounding material. Because the grating geometry and waveguide thickness cannot be precisely controlled in actual devices, α must be determined experimentally. Theoretical calculations of α are nonetheless very valuable to grating design, because they establish scaling relationships and design criteria that are needed for efficient grating fabrication. In addition, numerical evaluations of α for various geometries provide good measures of actual grating performance.

A theoretical analysis of thin etched groove grating couplers has been carried out[6] by using a perturbation approach.[17] In this case, the field equation is slightly modified by a small Δn^2 term, which is introduced by the presence of a periodic structure in the waveguide. Both analytic and numerical solutions have been obtained[6] by a linear combination of appropriate unperturbed modes. The grating coupling efficiency for several diffracted beams is, in general, given by

$$\eta = \eta_a F \quad \text{coupling from air} \tag{10}$$

$$\eta = \eta_s F \quad \text{coupling from substrate} \tag{11}$$

where η_a and η_s are given by Equation 34 of Reference 6 and involve the overlapping integral of the evanescent fields. F is the form factor as given by Equation 9.

The numerical values of η have been computed[18] for high resistivity GaAs epitaxial layers of different thickness grown on heavily doped n^+ GaAs substrate by using previously calculated β values[5] for the TE modes in these structures. Figures 12 and 13 show the typical plots of the computed optimum coupling efficiency as a function of the normalized groove depth, δ/λ, for a grating having a periodicity of 3.5 μm. The results represent only the case of forward coupling from air. The results for coupling efficiencies of higher order TE modes ($m > 1$) do not differ much in functional form from those computed for the TE_1 mode, except for the fact that the magnitudes of α_m vary significantly with m. It must be emphasized that Figures 12 and 13 represent the highest coupling efficiency, achievable only if the beam size R satisfies the condition $\alpha R = 0.625$.

In order to determine the optimum coupling length, computations of α_m must be made. Figure 14 shows the calculated $\alpha_m\lambda$ values as a function of grating groove depth as obtained by using Equation (21) of Reference 6. Figure 14 indicates that the optimum coupling length decreases with increasing mode order m, and groove depth δ. Furthermore, the optimum coupling length decreases with waveguide thickness, as shown in Figure 14. These results (Figure 14) are obtained for grating structure having a periodicity of 3.5 μm. These results further indicate that saturation occurs for δ/λ values near 0.1 for most cases. From Figure 3, we obtained the result that the optimum coupling lengths of the grating (optimum laser beam size for the case of forward coupling with a 3.5 μm periodic grating structure $2\alpha R = 2.43$, 3.01 and 15.90 mm for TE_0 mode in 10 μm, 20 μm and 30 μm thick waveguide respectively. In the case of TE_1 mode, the optimum coupling lengths are 0.87, 3.33 and 12.16 mm for 10, 20 and 30 μm, respectively. For most cases, it is desirable

FIG. 12

CALCULATED OPTIMUM COUPLING EFFICIENCY FOR THE TE_0 MODE OF GaAs/n+GaAs WAVEGUIDE, USING A 3.5 μm GRATING PERIODICITY

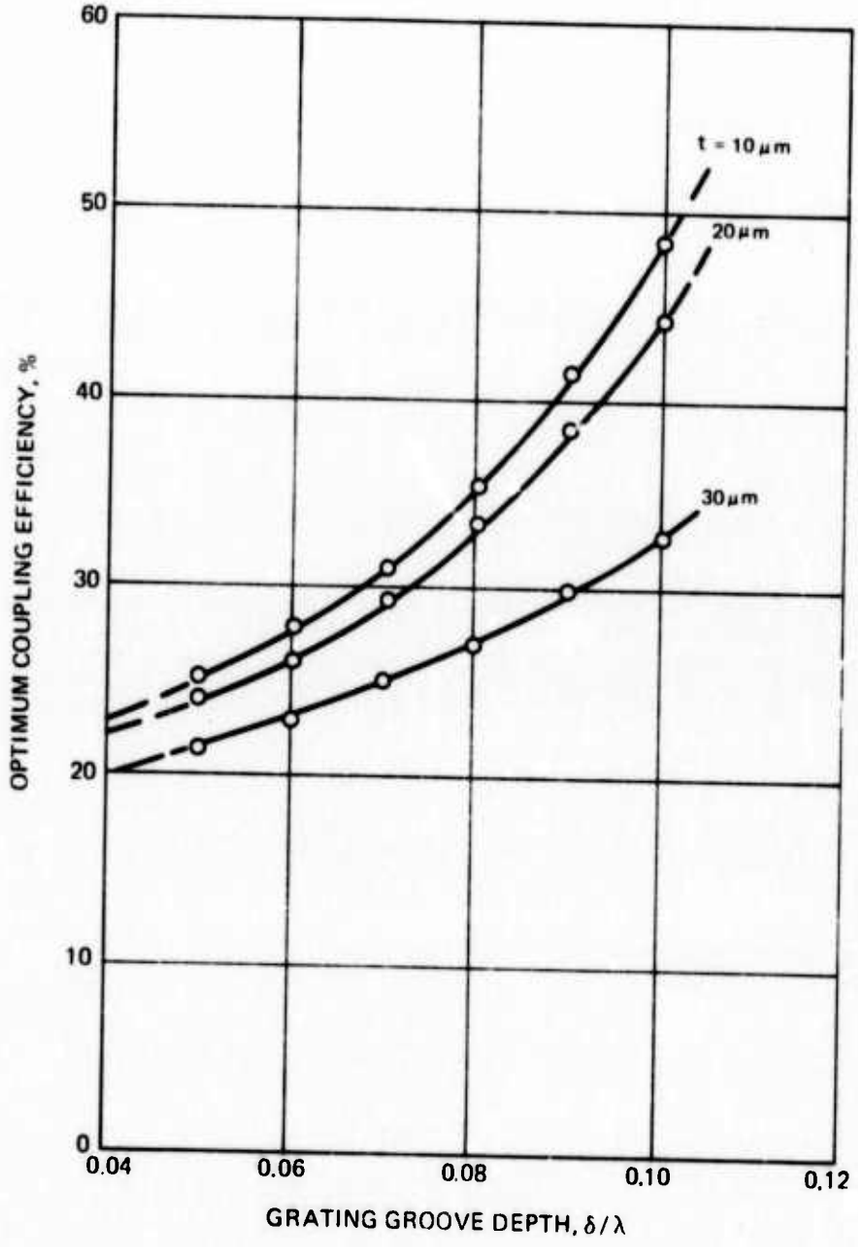

N03–82–1

FIG. 13

CALCULATED OPTIMUM COUPLING EFFICIENCY FOR TE_1 MODE OF GaAs/n^+ GaAs WAVEGUIDE, USING A 3.5 μm GRATING PERIODICITY

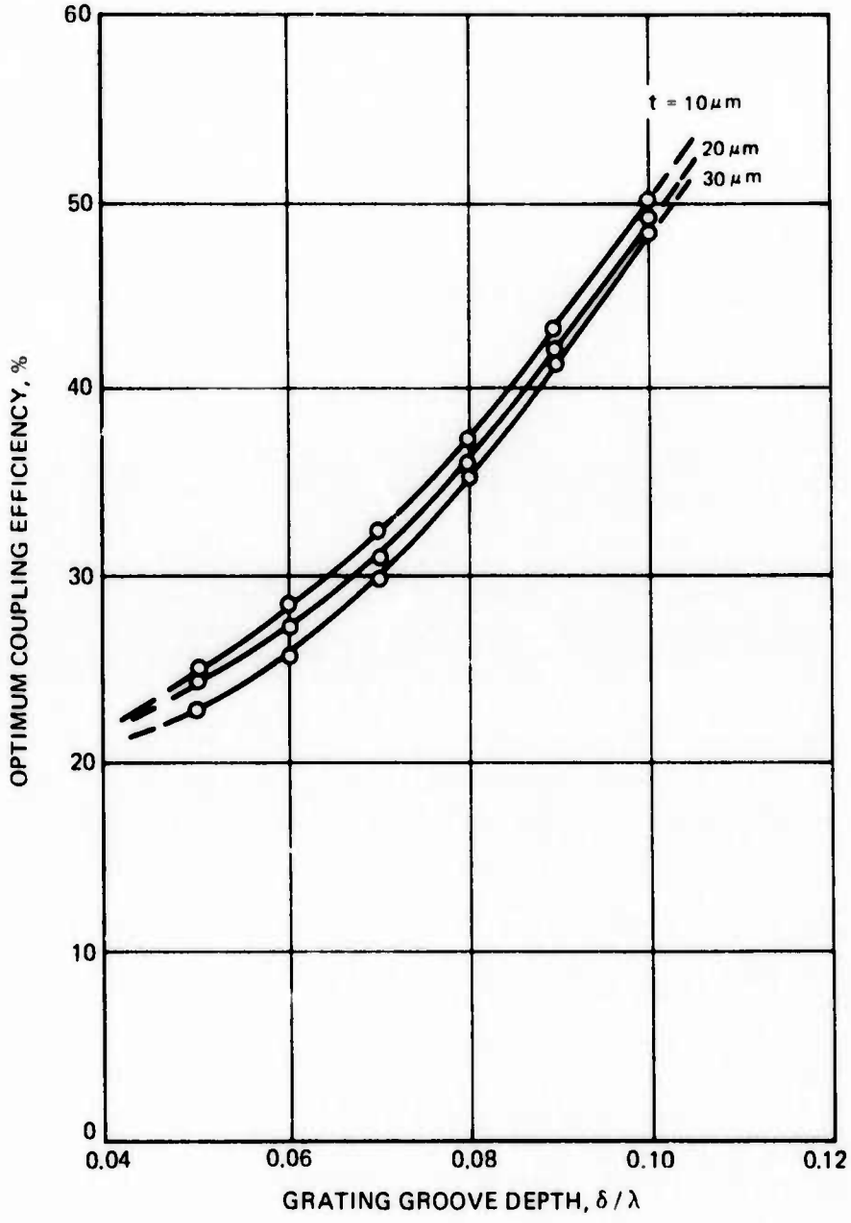

N03–82–2

FIG. 14

CALCULATED $\alpha_m\lambda$ VALUES vs GRATING GROOVE DEPTH δ/λ FOR A 3.5 μm GRATING PERIOD. λ = 10.6 μm; GaAs/n+ GaAs WAVEGUIDE STRUCTURE.

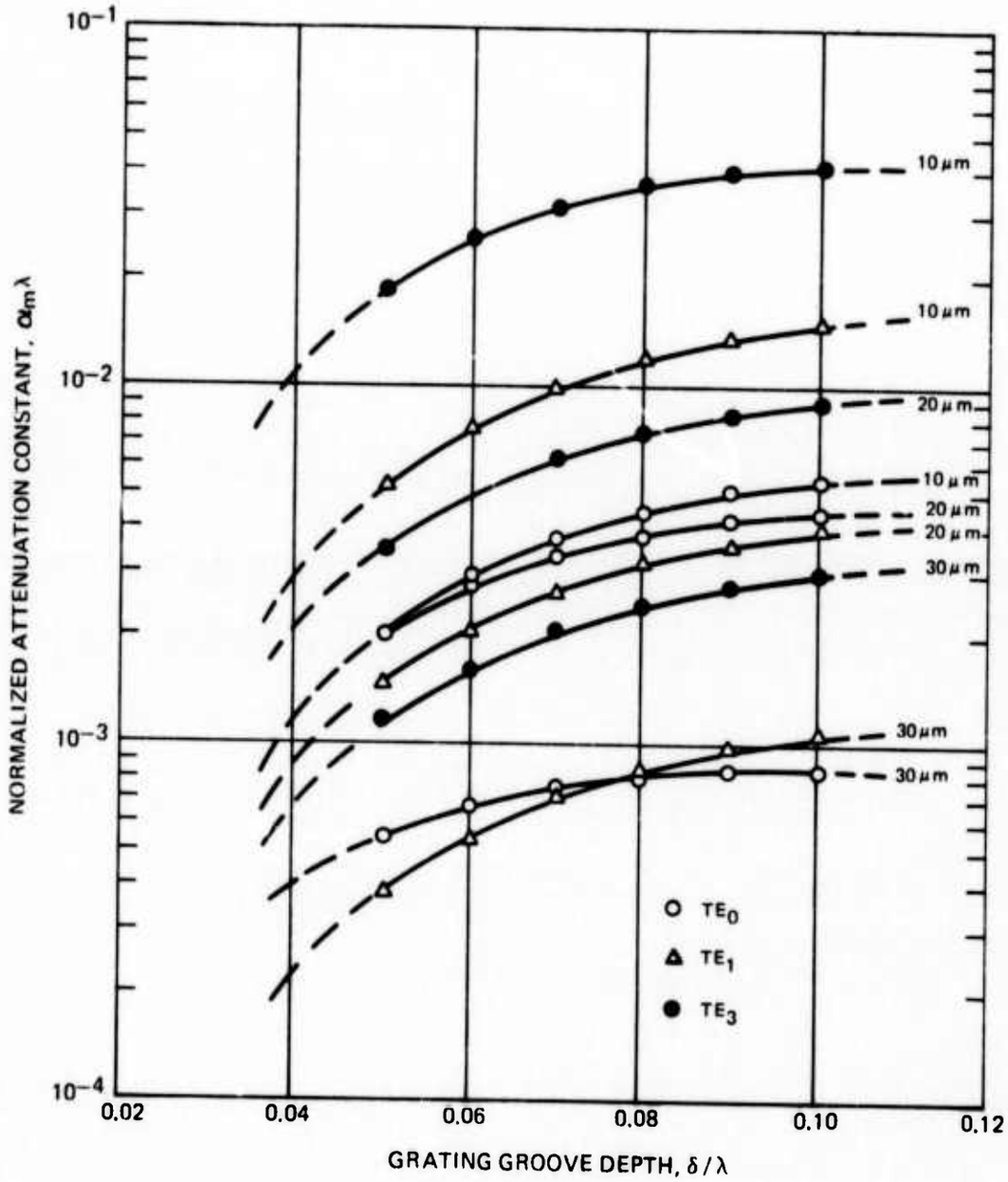

to work with a small laser beam size, e.g., $2R < 1$ mm. For these cases, forward coupling is not very efficient.

By means of backward coupling from the substrate, the theory[6] predicts that optical coupling efficiency as high as 81 percent can be obtained for all modes and all values of δ/λ. Obviously, this scheme is not applicable to n/n^+ GaAs waveguide because of the excessive absorption loss of 10 μm radiation in the n^+ substrate. However, other thin-films, e.g., the high resistivity GaAs or CdTe thin-films prepared by chemo-mechanical polishing can readily utilize this coupling scheme.

Figure 15 shows the calculated normalized attenuation constant $\alpha_m\lambda$ as a function of normalized groove depth δ/λ for a backward coupling of the CO_2 laser radiation by a 2 μm period grating. Calculation was made again for the TE modes in GaAs/n^+ GaAs, but the results provide useful information concerning the coupling characteristics of identical grating on the air/GaAs/air thin-film structure. The results of Figure 15 indicate that for optimum coupling, e.g., $\eta = 81\%$, the required laser beam size (or NA) is 0.65, 0.91 and 5.37 μm for the excitation of TE_o mode in 10, 20 and 30 μm thick GaAs/n^+ GaAs waveguide. Compared with values obtained for 3.5 μm period grating, these coupling lengths are considerably reduced.

Several factors are apparent from the results of Figures 12 to 15:

1. α varies with both the mode number of the surface wave and the waveguide thickness, being largest for higher-order modes and thin waveguides.

2. The variation of α with groove height δ saturates for $\delta > 0.2\ t$ where t is the waveguide thickness. As will be discussed below, the saturation effect may not be apparent for calculations that consider gratings which have been etched into the waveguide rather than deposited on it.

3. $\alpha\lambda$ can be as large as 10^{-2}. For $\lambda = 10.6\ \mu$ this value corresponds to $\alpha = 10\ cm^{-1}$. Even for such large values of $\alpha\lambda$, the inequality, $\alpha\Lambda << 1$, that is necessary for the validity of the leaky-wave model is well satisfied.

The variation of α with mode number can be qualitatively understood by a simple model that considers guided modes to consist of uniform beams that zig-zag through the waveguide and experience total internal reflection at the waveguide boundaries.[16] It can be shown that the mode propagation vector β_m is given by $(2\pi n_f/\lambda) \sin\theta$ where θ is the magnitude of the angle between the propagation direction of the bouncing wave and the normal to the waveguide (grating) plane. As the mode number m increases, θ decreases so that the beam experiences a larger number of bounces along a unit length. It is reasonable to expect that α should scale in the same manner as the number of bounces. Since the number of such bounces varies as $1/\sin\theta$, the relative values of α for different modes m and m' should be $\beta_{m'}/\beta_m$ and α should thus be higher, as found, for higher-order modes.

The observation that α increases with mode number is consistent with the fact that the normalized phase change Δ in Equation (7) increases with mode number. Such

FIG. 15

CALCULATED $\alpha_m \lambda$ VALUES vs GRATING GROOVE DEPTH δ/λ FOR A 2 μm GRATING PERIOD. $\lambda = 10.6\,\mu m$; GaAs/n^+ GaAs WAVEGUIDE STRUCTURE

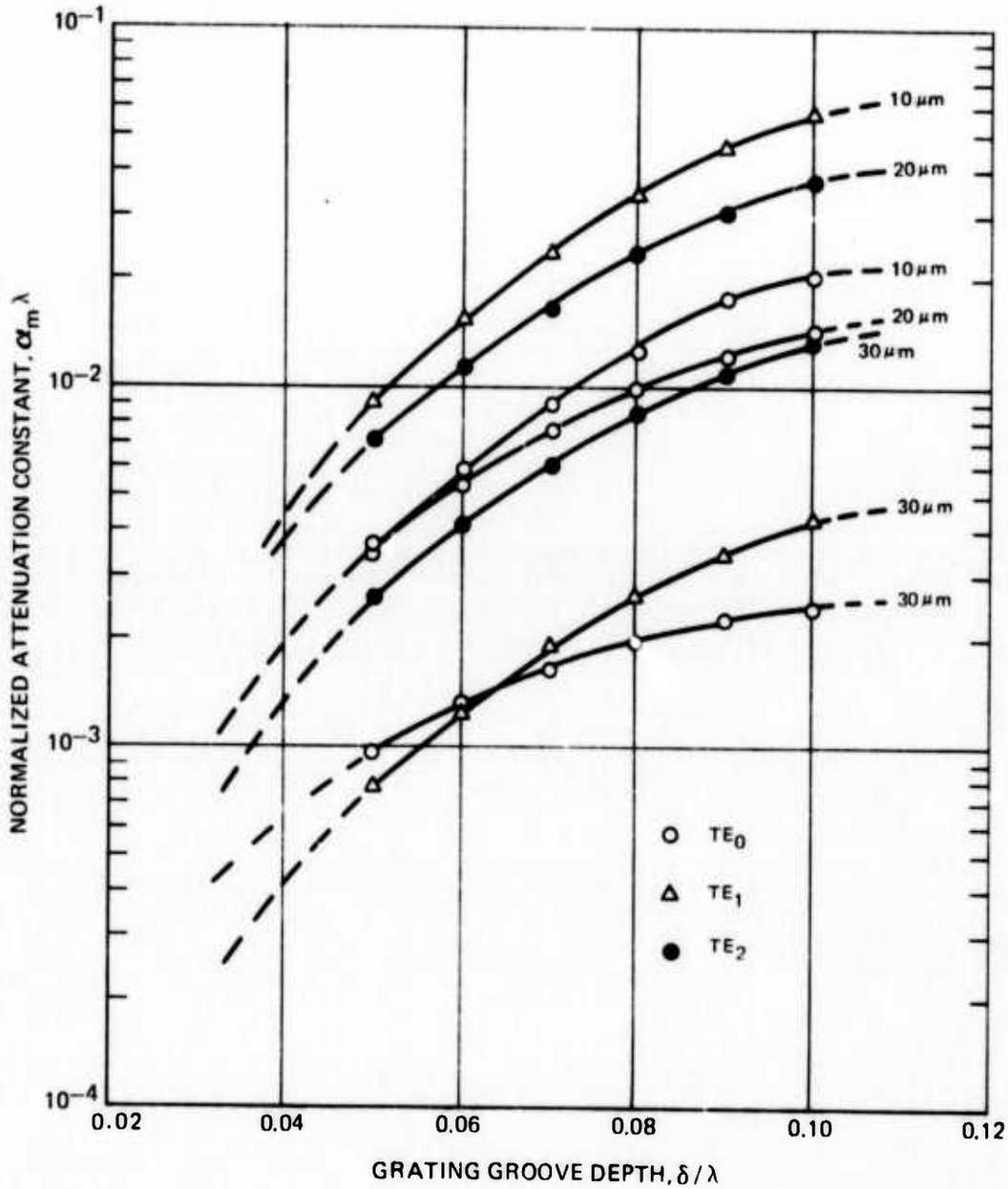

N03–82–4

a correlation is expected, because both Δ and α measure the degree of perturbations created by the grating. Δ also increases with decreasing waveguide thickness thus implying, as observed in Figures 14 and 15, that α increases for thin waveguides. Finally, the form of Equation 7 indicates that α can be large when there is a large index difference between the film and its surroundings. For such gratings, the range of value for $n-(\beta/k)^2$ is larger than for configurations in which the index difference between film and substrate is small.

The saturation of α with grating height is a consequence of the finite evanescent tailing of the leaky wave into the air region outside the grating.[11,19] It is well known in dielectric waveguide theory that the evanescent fields decay as $\exp(-pz)$, where $p = (k^2 - \beta^2)^{1/2}$ and z is the coordinate normal to the grating plane. Increasing the grating height to values much in excess of p, therefore, will not increase α beyond its maximum value because the fields drop rapidly to zero for $z > p$. (It can be shown that when $\Delta << 1$, p is not measurably changed by the presence of the grating). Because Tamir et al[11,19] considered only gratings that are deposited on top of a waveguide, they observed this effect for arbitrary grating geometries. Ogawa, et al[6] on the other hand, considered only gratings that are etched into a waveguide. For such configurations, saturation may not be reached because as the grating depth is increased, successively more intense portions of the leaky beam are encountered and the perturbation quickly becomes invalid. Although some degree of saturation is seen in Ogawa's calculations in Figures 14 and 15, similar calculations for other waveguide configurations[6] do not show this effect.

The saturation of α with grating height is well described by the factor $[1 - \exp(-D\delta)]$ where D is a parameter of order p.[19] For small δ, then, α should scale as δ^2. Such scaling can be shown to be consistent with the performance of bulk phase gratings[20] and is, in fact, predicted for thin-film phase gratings.[19]

Another scaling relationship for α that may be useful for grating fabrication is $\alpha \sim 1/\Lambda$ where Λ is the grating period. For fixed groove geometry and waveguide characteristics, therefore, $\alpha\Lambda$ is constant. This relationship is a mathematical consequence of the physical observation that α should be proportional to the number of scattering centers (grating grooves) per unit length. In particular, since the power in a leaky wave changes as $dp/dx = -2\alpha P$,

$$\frac{dP}{dx} \approx -\frac{P^S cell}{\Lambda} = -2\alpha P$$

so that

$$\alpha\Lambda = \frac{P^S cell}{p} = a_o. \qquad (12)$$

$P^S cell$ is the absolute scattering loss for each scattering center and is equal to a scattering efficiency a_o times the incident power P at the scattering center.

These various scaling relationships for α allow us to extrapolate measurements of α made for a particular mode, film thickness, and grating depth to other conditions. Although these extrapolations are only semiquantitative at best, they

nonetheless serve as useful guides for grating construction.

4.4 Grating Optimization

As discussed in Section 4.2, grating diffraction efficiency can be as high as 80 percent for a uniform input grating if the input beam size is adjusted to match the coupling coefficient α. Output coupling efficiency can always be made arbitrarily close to 100% by simply increasing the output grating length. In principle, then, a uniform grating pair can transmit up to 80 percent of the incident light provided care has been taken to allow only a single diffracted order.

In addition to transmitted power, there are those other considerations that can be of substantial practical importance to thin-film modulator design. The first consideration is that the physical dimensions of the grating and out-coupled beams should be as small as possible. Secondly, the angle $|\theta|$ in Equation 1 should be kept small. This latter requirement can be shown to offer advantages for the construction of the modulator frame as well as easing fabrication constraints because it allows the grating period to be increased. Finally, for many applications it is highly desirable that the intensity distribution of the output beam be close to a truncated Gaussian rather than the exponential form in Figure 9. In this section, we discuss how a grating pair with high-peak transmission can be optimized in terms of these three considerations.

Grating size is minimized when α is made as large as possible. The results of Section 4.3 indicate that α is largest for higher-order modes, thin waveguides, large index differences between film and air, and grating depths of order p where p is typically $\sim$ 0.1 t. Because a metal substrate may be needed in order to prevent extra diffracted beams, however, waveguide attenuation in the modulator waveguides can become significant when high-order modes and thin waveguides are used. As a result, α cannot be increased to its maximum value. Analysis of the behavior of the GaAs modulator indicates that use of TE_0 or TE_1 propagation in a 20 μ guide is optimum.[5] Under these conditions, α is constrained to values of no more than about 3 cm^{-1}. Such values can be achieved by etching a symmetric grating about 2 μ deep into the GaAs wafer. Results from Reference 8 suggest that the grating should be placed on the substrate side, in contact with the metal film, so that the difference in index of refraction between the grating and its surroundings is as large as possible.

The groove period Λ should be chosen so that only first-order backward diffraction can occur. This prescription, which was noted in Section 4.3 does not indicate whether large or small values of $|\theta|_{inc}$ are desirable. As already noted, the design and fabrication of both the grating and the modulator frame are somewhat simplified if near-normal incidence and consequently larger values of grating period can be used. However, the use of near-normal incidence involves certain trade-offs. In particular, we now show that when $|\theta|$ in Equation 1 is decreased, the length of grating needed for optimum coupling decreases somewhat whereas the optimum size of the input laser beam (as measured perpendicular to its propagation direction) decreases.

Consider two input gratings that are identical in every feature except one. The first grating has a period Λ_1, chosen so that backward coupling occurs at $\theta_{inc} = \theta_1$. Backward coupling for the second grating with period $\Lambda_2 < \Lambda_1$ occurs at an angle $\theta_2 > \theta_1$. (See Figure 16). We will show that the radius ω_1 of the optimum-size Gaussian beam for the first grating is somewhat smaller than ω_2. On the other hand, the sizes of the projections $\omega_{1,x}$ and $\omega_{2,x}$ on the grating surface are such that the input grating for case 2 can be made somewhat smaller than the grating for case 1.

As discussed in Section 4.2, input coupling is optimized for a uniform grating when $\omega_{1,x}\ \alpha_1 = \omega_{2,x}\ \alpha_2 \approx 0.6$ to 0.7 with the exact value depending on the input beam intensity distribution. Therefore,

$$\frac{\omega_{1,x}}{\omega_{2,x}} = \frac{\alpha_2}{\alpha_1} \tag{13}$$

It was shown in Equation 12 that $\alpha\Lambda$ is a constant a_o for given groove geometry and waveguide configuration so that $\alpha_2/\alpha_1 = \Lambda_1/\Lambda_2$. The grating periods Λ_1 and Λ_2 can be related to the angles of incidence by using the grating equation for first-order backward diffraction. From Equation 1 with the present convention on the sign of θ

$$\frac{1}{\Lambda} = \frac{1}{\lambda}\,(\beta/k + \sin\theta). \tag{14}$$

Combining Equations 13 and 14 gives the important result, for the ratio of grating length as

$$\frac{\omega_{1,x}}{\omega_{2,x}} = \frac{\beta/k + \sin\theta_2}{\beta/k + \sin\theta_1}\ . \tag{15}$$

Since $\omega_x = \omega/\cos\theta$, the ratio of incident beam sizes is

$$\frac{\omega_1}{\omega_2} = \frac{\cos\theta_1\,(\beta/k + \sin\theta_2)}{\cos\theta_2\,(\beta/k + \sin\theta_1)} \tag{16}$$

Equation 15 is larger than unity whenever $\theta_1 < \theta_2$. As a result, a longer input grating is needed for optimum coupling at smaller angles of incidence. It can be shown from Equation 16, on the other hand, that decreasing θ decreases the optimum size of the input beam. In order to qualify these trends, we consider $\theta_1 = 10^\circ$ and $\theta_2 = 45^\circ$ for the TE_1 mode of the GaAs wafer ($\beta/k \approx 3.25$). These angles of incidence are appropriate for grating periodicities of 3.1 μ and 2.7 μ, respectively. From Equation 15, the ratio of grating lengths ($\omega_{1,z}/\omega_{2,z}$) is found to be 1.15 and from Equation 16 the ratio of beam size is 0.83. If the angle of incidence is decreased from 45° to 10°, therefore, the grating length required for optimum coupling is increased by 15 percent whereas the optimum size of the incident laser beam as measured along the propagation direction is decreased by 17 percent.

FIG. 16

INPUT COUPLING FOR TWO GRATINGS WHICH DIFFER ONLY IN GRATING PERIODICITY

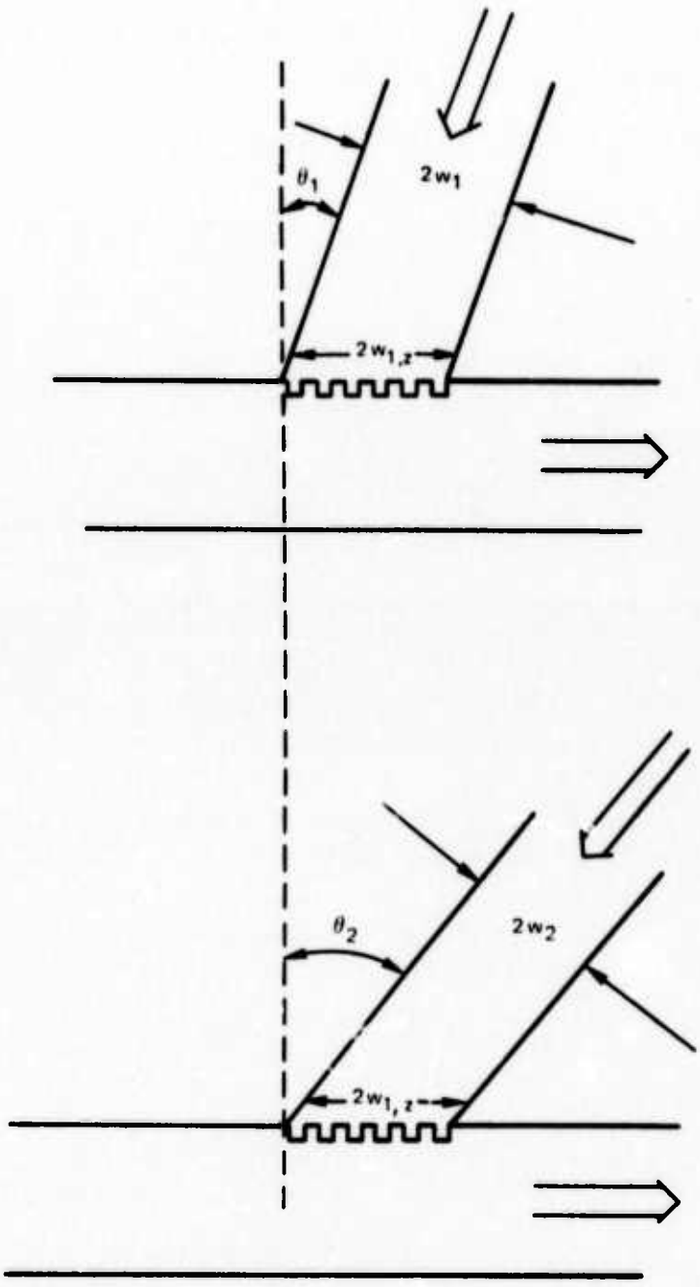

N03–255–1

Grating size is a far more important experimental consideration than beam size. Consequently, the present analysis indicates that there is a disadvantage to near normal incidence that must be weighed against the advantages gained in relaxed grating tolerances and modulator frame design.

The last type of optimization to be considered in this section is beam profile tailoring. The basic problems involved can be appreciated by considering the profile of the light beam coupled out of a waveguide by a uniform grating. Many applications require a more symmetric beam than shown in Figure 9. In particular, a truncated Gaussian distribution is normally desired. By fabricating nonuniform gratings that are characterized by an attenuation coefficient that varies with x, it is possible to tailor the output intensity distribution in the x direction to match virtually any functional form desired. (The intensity distribution in the y direction is the same as the corresponding profile of the input beam.) Such tailoring, in addition to improving the form of the coupled output beam, can also be used to increase the coupling efficiency for an input grating to 100 percent if $E_a(x)$ in Equation 8 is made to exactly match $E_{in}(x)$.

α has been tailored for a prism coupler by creating a linear taper on the prism-waveguide gap[16]. Because α varies linearly with the size of the gap, the tapered prism coupler is equivalent to a generalized coupler with $\alpha = \alpha_o x$. A theoretical coupling efficiency of 96 percent was calculated and 88 percent actually measured. This same linear variation in α can be achieved with a grating by varying the groove depth in an appropriate manner.

We have calculated the near-field intensity for a grating or prism coupling characterized by a linear attenuation coefficient by using Equation 6 and have compared the resulting function to a best-fit truncated Gaussian. As seen in Figure 17, the match between the curves is reasonable. A better match can be made by either considering a Gaussian with smaller truncation at x - 0 or by allowing the tailored beam to propagate to the far-field.

An exact match in the near-field can be made by solving the equation.

$$E_a(x) = E_G(x) \tag{17}$$

for $\alpha = \alpha_G(x)$. $E_a(x)$ is defined by Equation 6 for $x > 0$, and $E_G(x)$ is a Gaussian function that peaks at $x = x_m$ and has the form

$$E_G(x) = A \exp\left[-(x-x_m)^2/\sigma\right], \tag{18}$$

Both functions vanish for $x < 0$. The amplitude A and the beam width σ are constants. Equation 17 can be solved most conveniently by squaring both sides. After some manipulation we find

$$\alpha_G(x) = \frac{1}{2} \frac{\exp\left[-2(x - x_m)^2/\sigma^2\right]}{\int_x^\infty \exp\left[-2(x' - x_m)^2/\sigma^2\right] dx'} \tag{19}$$

FIG. 17

COMPARISON BETWEEN A TRUNCATED GAUSSIAN AND $(E_a)^2$

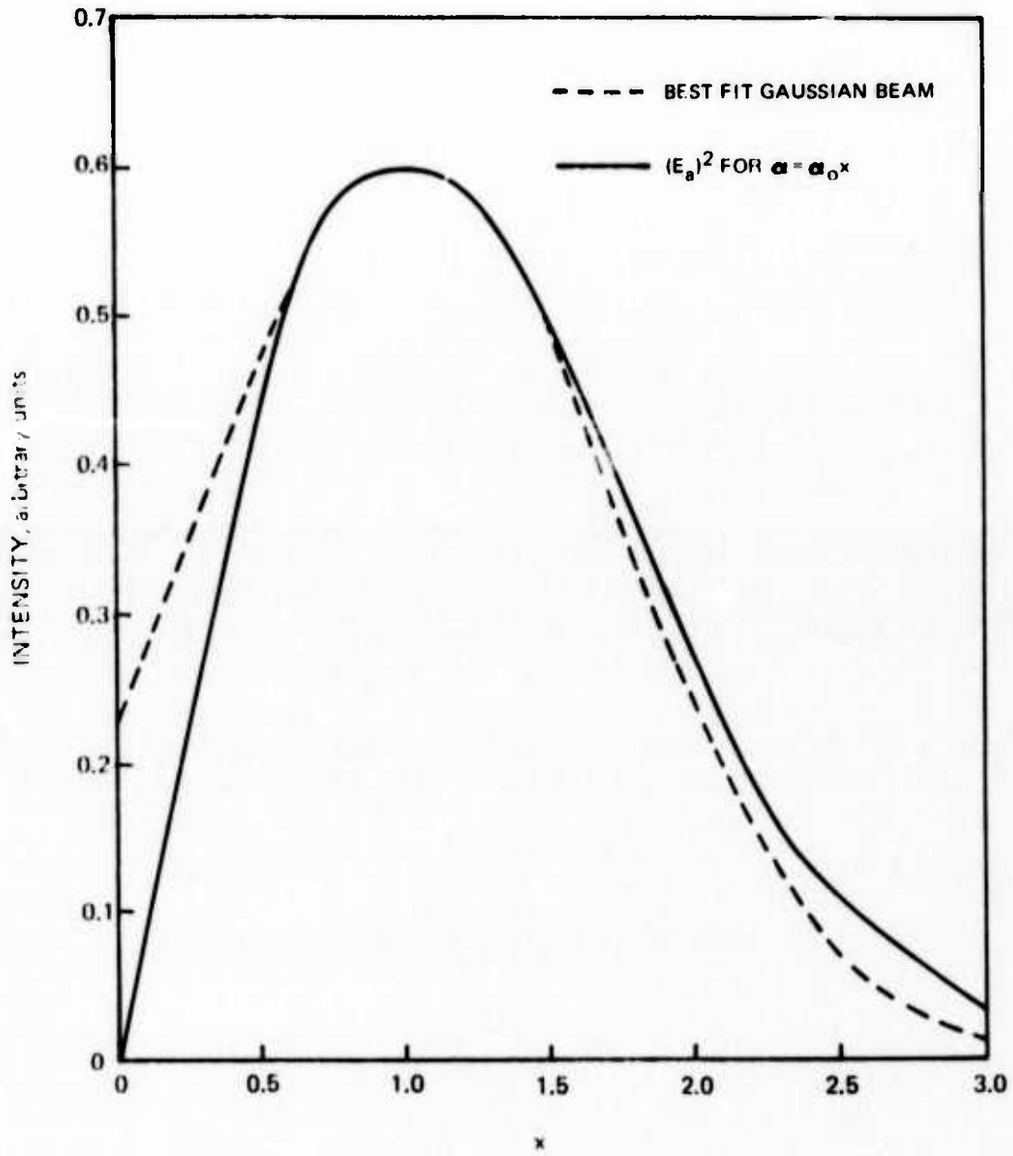

N03–225–2

For small x, $\alpha_G(x)$ is essentially constant, and for large x, the asymptotic expansion of the complimentary error function in the denominator leads to $\alpha_G \sim x$.

If the attenuation constant in Equation 19 can be implemented in practice by proper control and variation of groove depth, the resulting grating will produce a perfect truncated Gaussian in the near-field when it is used as an output coupler. If such a grating is used as an input coupler and irradiated by a beam that has the precise form of Equation 18, a theoretical input coupling efficiency of 100 percent can be achieved. Calculations are now underway to relate $\alpha_G(x)$ to a variation in groove depth with distance as well as to characterize the match between a Gaussian and the output beam of Figure 17 in the far-field.

In conclusion, we have considered several aspects of grating coupler optimization. Because of various design constraints, it is not possible to increase α to its maximum values or to reduce the grating length to minimum values. Certain trade-offs that are possible in modulator design have been discussed in this section. The tailoring of output gratings to produce Gaussian output beam has been treated analytically. Although analysis indicates that, in principle, beam tailoring causes no difficulties, the experimental realization of grating tailoring may require considerable effort.

5.0 Microwave Mini-Gap Ridge Waveguide Structure

5.1 Introduction

The previous report[8] describes in detail the approach selected for obtaining a waveguiding structure that will serve for propagation of both the laser and the microwave energy. For efficient optical modulation in the GaAs structure, the microwave energy must be confined to the small cross-section occupied by the guided laser beam. It is also required that the phase velocity of microwave energy in the transmission line be the same velocity as that of the optical beam. The cross-section of the interaction region was selected to be 1.0 millimeters wide and 25 microns high where the top and bottom surfaces of this waveguide structure are conducting metal surfaces. This region, then, forms the complete optical waveguide while for the microwave frequencies, this region serves as the gap of a mini-gap ridge waveguide.

Application of the mini-gap ridge waveguide, initially at X-band frequencies required measurements of the electrical parameters of the structure. It was determined that the GaAs-filled ridge had a characteristic impedance of 5 ohms and that the effective index refraction of the medium was approximately 3.1, as compared to a value of 3.3 expected for a homogenous waveguide filled with GaAs. The microwave properties of the line were determined from measurements on terminated and open circuited resonant sections. Similar determinations were carried out for air-filled gaps to provide data for the broadband designs. A useful and somewhat unique characteristic of the mini-gap ridge waveguide structure is the technique used to couple to the mini-gap ridge waveguide from a 50 ohm coax line. By making the transition region quite small compared to microwave wavelengths, it was possible to obtain efficient broadband transitions that should be useful up to at least 17 GHz. The present measurements of the mini-gap ridge waveguide characteristics will only serve as an approximate guide in designing the final broadband modulators, because the parameters of the optical waveguide are not yet fully determined and, also, because the dimensions are so small that it is difficult to make reproducible structures.

A particular useful result presented in the previous report[8] was that lengths of ridgewave guides operating as resonators provided impedances of nearly 50 ohms at their terminals. Because of this fact, the structure could be used as a resonant modulator without any additional impedance matching. During this reporting period, trade-offs between the traveling-wave structure and the resonant structure were analyzed to determine if the resonant structure could be used to improve the efficiency of modulation. This comparison was made without regard to bandwidth. Because it was simple and direct to build a resonant structure at X-band that included synchronization of the waves, such a structure was built and used for the successful modulation experiments (Section 2).

The microwave work was shifted to the 16 GHz range during this period so that broadband matching, which would require a certain amount of emperical adjustment, could be performed directly at the desired frequencies. The short-term goal is 500 MHz of bandwidth. Eventually, bandwidths in excess of 1500 MHz should be possible. An experimental model of a wideband modulator was constructed. It was used both

for determining the parameters of the mini-gap ridge waveguide structure and for working out a preliminary structure for broadband impedance matching of 50 ohms to the GaAs filled mini-gap.

5.2 X-Band Resonant Modulator

An X-band resonant modulator was designed and evaluated. The resonant condition was selected because of the enhanced efficiency with which power is generated in the sidebands by phase shift modulation and the ease of impedance matching with this design. The sideband power, itself, is proportional to the $(\Delta\phi)^2$, where $\Delta\phi$ is the maximum amplitude of the phase shift deviation. Before proceeding with the discussion of the experimental work, the maximum phase deviation for traveling wave and resonant structures will be compared and, in addition, synchronization techniques will be discussed.

Several cases of optical phase modulation in a microwave transmission line - one with a traveling wave and the others with standing waves - are depicted in Figure 18. In the first case, assume that the maximum available power is delivered to a traveling wave and that the transmission line is terminated in its characteristic impedance. Then the voltage in the traveling wave is given by $V_i = (PZ_o)^{1/2}$ where P is the maximum available power and Z_o is the characteristic impedance of the modulator line($Z_o \simeq \xi\frac{h}{W}$) (Figure 18a). If we assume that a synchronous condition exists between the microwave and the guided laser beam, then the maximum total accumulated phase deviation is given by

$$\Delta\phi = \frac{\gamma}{h}\int_o^L V_i e^{-\alpha} dx \qquad (20)$$

where $\gamma = \pi/\lambda$, $r_{41} \simeq 1.2 \times 10^{-10}$ m/V, α is the microwave wave attenuation constant and h is film thickness. Evaluation of this expression yields

$$\Delta\phi = \gamma L \left(\frac{P\xi}{hW}\right)^{1/2}\left(\frac{1-e^{-\alpha L}}{\alpha L}\right). \qquad (21)$$

For smaller attenuation, reduces to

$$\Delta\phi \simeq \gamma L \left(\frac{P\xi}{hW}\right)^{1/2}\left(1 - \frac{\alpha L}{2}\right), \qquad (22)$$

for $\alpha L < 0.1$. Thus, the total or net phase deviation is linearly proportional to the modulator length, the square root of power, and the inverse of the cross-sectional area. The latter emphasizes the importance of maximizing the microwave power density in the modulator. The maximum possible value for phase deviation that occurs for large values of L, and consequently for large αL, is

$$\Delta\phi \simeq \gamma \left(\frac{P\xi}{hW}\right)^{1/2}\frac{1}{\alpha}, \qquad (23)$$

which is valid for $\alpha L > 2$.

CIRCUIT MODELS OF MODULATOR

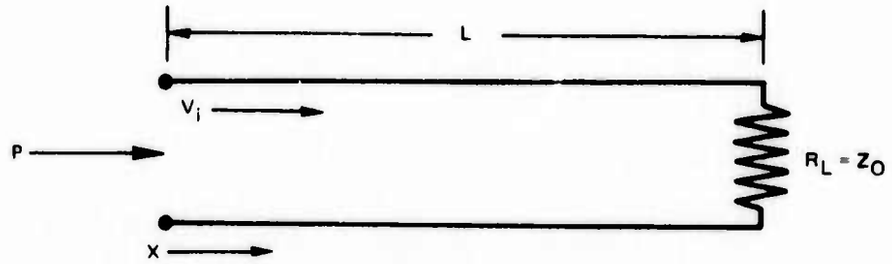

a) TRAVELING WAVE

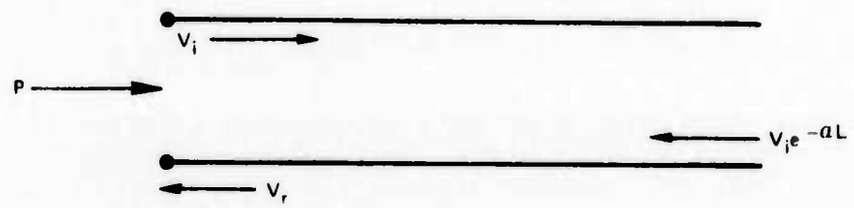

b) STANDING WAVE

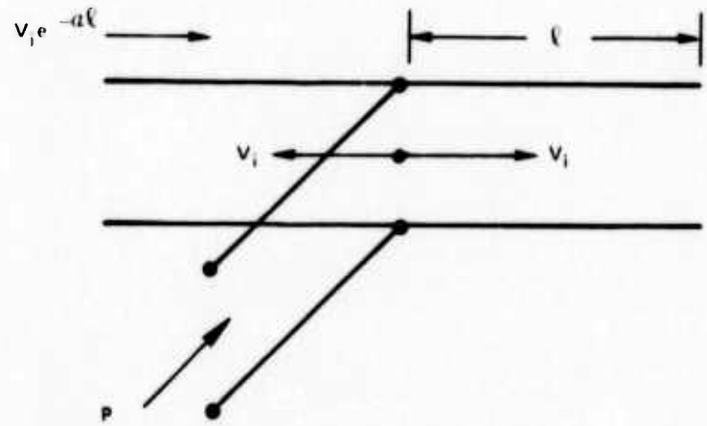

c) TRANSVERSE FED RESONATOR

Therefore, $\Delta\phi$ is limited only by the attenuation coefficient once αL exceeds approximately 2 (i.e., for a total attenuation of 17 dB).

The second case of interest - the standing wave modulator (Figure 18b) - consists of an open-circuited transmission line that is strongly coupled to a source and, consequently, delivers maximum power. The line is a multiple of $\lambda/2$ in length and the microwave power is dissipated in the line losses. By using this design, high values of electric field are developed but the operating bandwidth is reduced. Again we assume that the synchronous condition is satisfied. Accumulative interaction with the guided laser beam only occurs for the forward component of the standing wave.

For this lossy resonant transmission line, the input shunt resistance at resonance is

$$R = Z_o \frac{1 + e^{-2\alpha L}}{1 - e^{-2\alpha L}} \tag{24}$$

and the terminal voltage for the matched condition is $V = (PR)^{1/2}$ where P is the maximum available power from the driving source. Because a standing wave exists, the amplitude of the incident wave at the input terminal is

$$V_i = \frac{V}{1 + e^{-2\alpha L}} \tag{25}$$

Introducing expressions 24 and 25 into Equation 20, the accumulated phase deviation becomes

$$\Delta\phi = \gamma L \left(\frac{1 - e^{-\alpha L}}{\alpha L}\right) \left[\frac{P\xi}{hW (1 + e^{-2\alpha L}) (1 - e^{-2\alpha L})}\right]^{1/2} . \tag{26}$$

For small values of attenuation, the expression for phase deviation becomes

$$\Delta\phi = \frac{\gamma}{2}\left(\frac{P\xi L}{hW\alpha}\right)^{1/2}\left(1 + \frac{\alpha L}{2}\right), \tag{27}$$

which is valid for $\alpha L < 0.1$. In this limit, the phase modulation only increases with $(L)^{1/2}$.

The above analysis can be extended to the case where the modulator is center-fed (Figure 18c) so that the distances from the feedpoints to the ends are $\ell = L/2$. Because the section is center-fed and significant microwave attenuation frequently exists, the arm at which the light enters will provide less modulation than the arm from which light leaves. Letting P still equal the total input power to the modulator and modifying Equation 26 so as to apply it to each of the arms, the maximum phase deviation.

$$\Delta\phi = \gamma\left(\frac{P\xi}{2hW}\right)^{1/2}\left[\frac{(1 - e^{-\alpha\ell})(1 + e^{-\alpha\ell})}{\alpha\ell\ (1 - e^{-2\alpha\ell})(1 + e^{-2\alpha\ell})^{1/2}}\right]. \tag{28}$$

For small attenuation, $\Delta\phi$ becomes

$$\Delta\phi \simeq \frac{\gamma}{2}\left(\frac{P\xi L}{hW\alpha}\right)^{1/2}. \tag{29}$$

From Equations 28 and 29, we note that, as before, increasing the length of the modulator generally increases the degree of modulation. No significant difference is found from the preceding case.

It is important to compare the phase deviation for the traveling wave modulator to that of the standing wave modulator for the same available microwave power. The exact ratio of phase deviations from Equations 21 and 26 is

$$\frac{\Delta\phi_{SW}}{\Delta\phi_{TW}} = (1 - e^{-4\alpha L})^{-1/2}. \tag{30}$$

This ratio is always larger than unity and becomes, for $\alpha L \ll 1$

$$\frac{\Delta\phi_{SW}}{\Delta\phi_{TW}} \simeq \frac{1 + \alpha L}{2(\alpha L)^{1/2}}. \tag{31}$$

Since the sideband power is proportional to the square of the maximum phase deviation, Equation 31 shows that the standing wave case gives greater efficiency than the traveling wave configuration but at the expense of bandwidth. As an example, a resonant line having 2 dB attenuation can provide 67 percent more sideband power than a traveling wave line - for 3 dB attenuation, 33 percent more power is provided.

Effective operation of the modulator requires that a synchronous condition exist between the microwave and the guided 10.6 micron beam. Because a certain amount of microwave energy exists in the surrounding air, the microwave propagation velocity is larger than that for waves traveling exclusively in the gallium arsenide. As a result, a technique is introduced to reduce the microwave velocity.

A common technique for reducing the microwave velocity is to introduce periodic discontinuities along the transmission line. For the ridge guide, this can be accomplished by introducing changes in the characteristic impedance of the line as shown in Figure 19a. The periodic microwave structure is designed with a period of $v_\ell/2f_\mu$ where v_ℓ is the propagation velocity of the 10.6 micron beam and f_μ is the microwave frequency. The required changes in characteristic impedance can be achieved with steps in the gap height or removal of material from the side of the ridge as illustrated in Figures 19b and 19c. Such periodic structures act also as filters with dispersion. Consequently, it will be necessary to examine the effects of dispersion on the synchronous condition in order to establish ultimate bandwidth

FIG. 19

TECHNIQUES FOR SYNCHRONIZATION

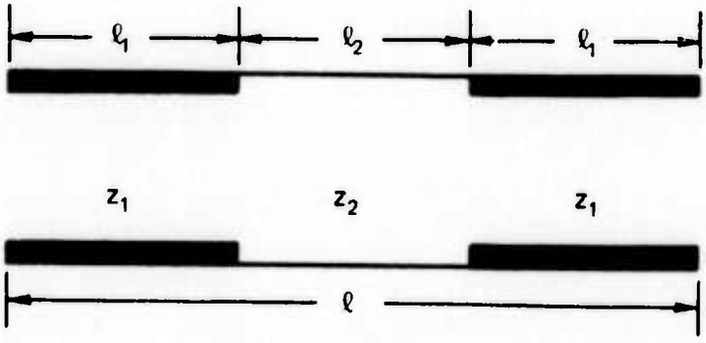

a) CIRCUIT MODEL

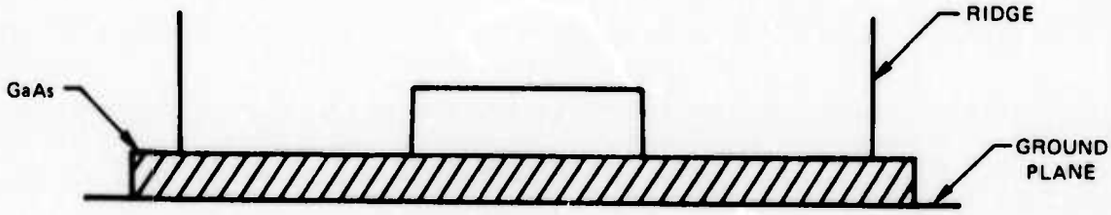

b) STEPPED RIDGE

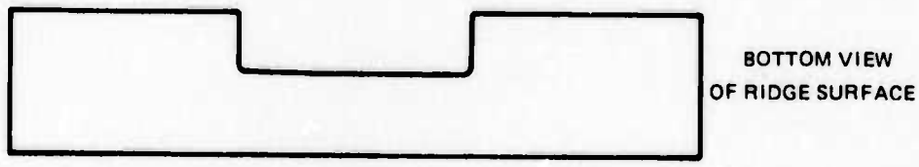

c) THINNED RIDGE

limitations. Fortunately, only a limited number of sections are to be used so that a large reduction in modulation efficiency should not occur with this technique.

The periodic modulating structure will also result in a reduction of efficiency due to the fact that the microwave field will no longer be a simple sinusoid along the modulating region. A section of stepped ridge waveguide and the corresponding electrical field distribution in the various sections of the ridge are shown in Figure 20. Note that the fields are largest in the narrow gap region. A well-known method for analyzing this type of problem is to decompose the electric field distribution into spatial harmonics. By design, the first spatial harmonic structure will have the required velocity for synchronism with the 10.6 micron beam. The higher-order spatial harmonics will travel with velocities that are multiples of the synchronous velocity and, therefore, will have a relatively small effect on the ir beam. Thus, the amplitude of the first spatial harmonic determines the maximum value of phase modulation. The amplitude of the first spatial harmonic is smaller than the maximum field that exists in the modulator and, therefore, a certain loss in modulation efficiency will result because of the periodic nature of the structure. This effect is not large enough to seriously reduce the modulation and will not be considered further at this time.

Of the two techniques considered for synchronization of the waves, the thinned section is preferred over the step, because in the process of assembling the structure, it is necessary to establish a co-planar condition between the surface of the ridge and the two supporting arms by polishing the structure on a flat surface. Removing metal by polishing alters the height of a step in the ridge and thereby changes the properties of the structure. Polishing does not alter the properties of a thinned ridge, however.

Consider, again, the X-band experiments. A sketch of the resonant X-band modulator structure is shown in Figure 21. The full length of the structure was equal to one microwave wavelength (0.9 cm), which was equal to v_ℓ/f_μ. Allowance was made for the effects of the fringing fields. The ridges were thinned at the points of maximum current in order to lower the resonant frequency to the selected operating frequency of 10 GHz. Thus, synchronization was also obtained in the standing wave structure. The feedline perpendicular to the resonant structure was designed to be a 50 ohm ridge section in accordance with experimental results for the air-filled ridge as discussed in the previous report.[8] The slice of GaAs containing the optical grating couplers was fit between the ridge and the ground plane. The resonant ridge represented a resistive load of approximately 30 ohms. Most of the energy was, thus, transferred into the resonant structure and produced the desired modulation. The value of the voltage amplitude of the forward wave synchronous with the optical wave was estimated to be 17.5 volts for 20 watts of incident power. Figure 22 is a photograph of the disassembled modulator.

5.3 Ku-Band Broadband Modulator

The microwave activities have been shifted during this period to the 16 GHz range in order to start work on the final broadband structure. Experiments similar

EFFECTIVE MODULATING FIELD IN STEPPED GAP

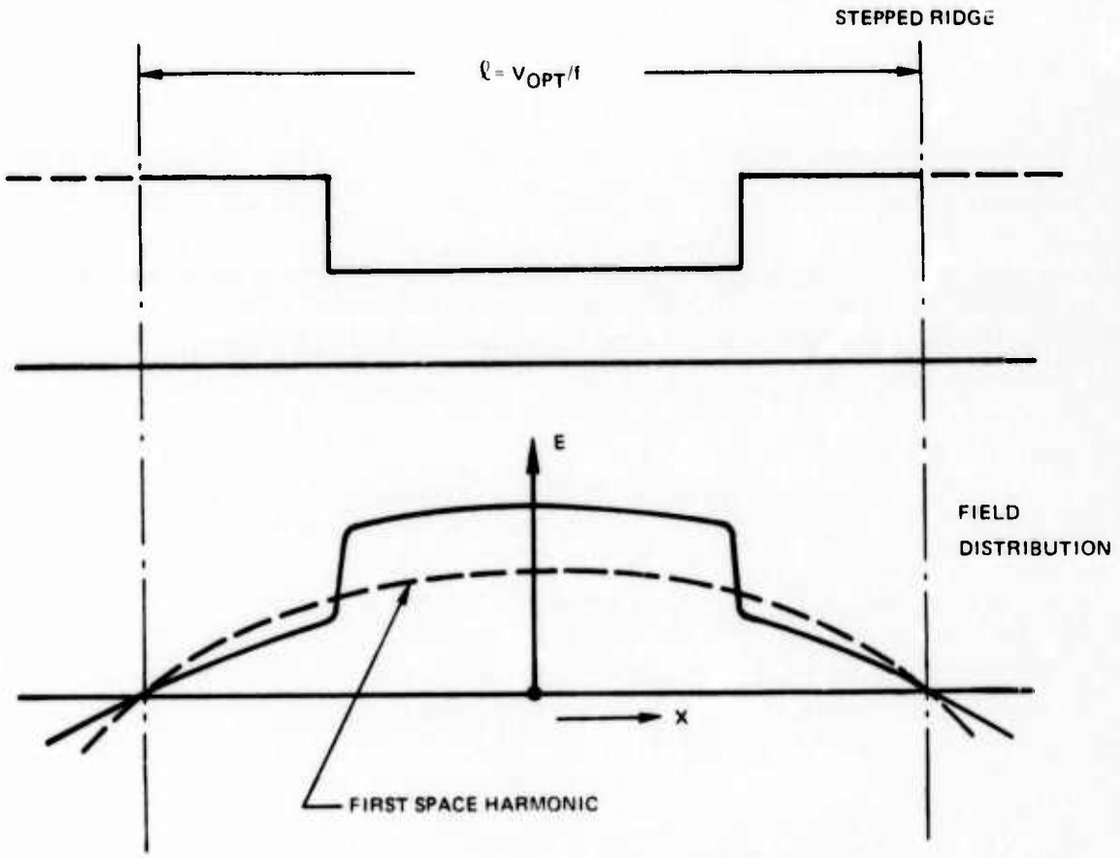

FIG. 21

SKETCH OF RESONANT MODULATOR

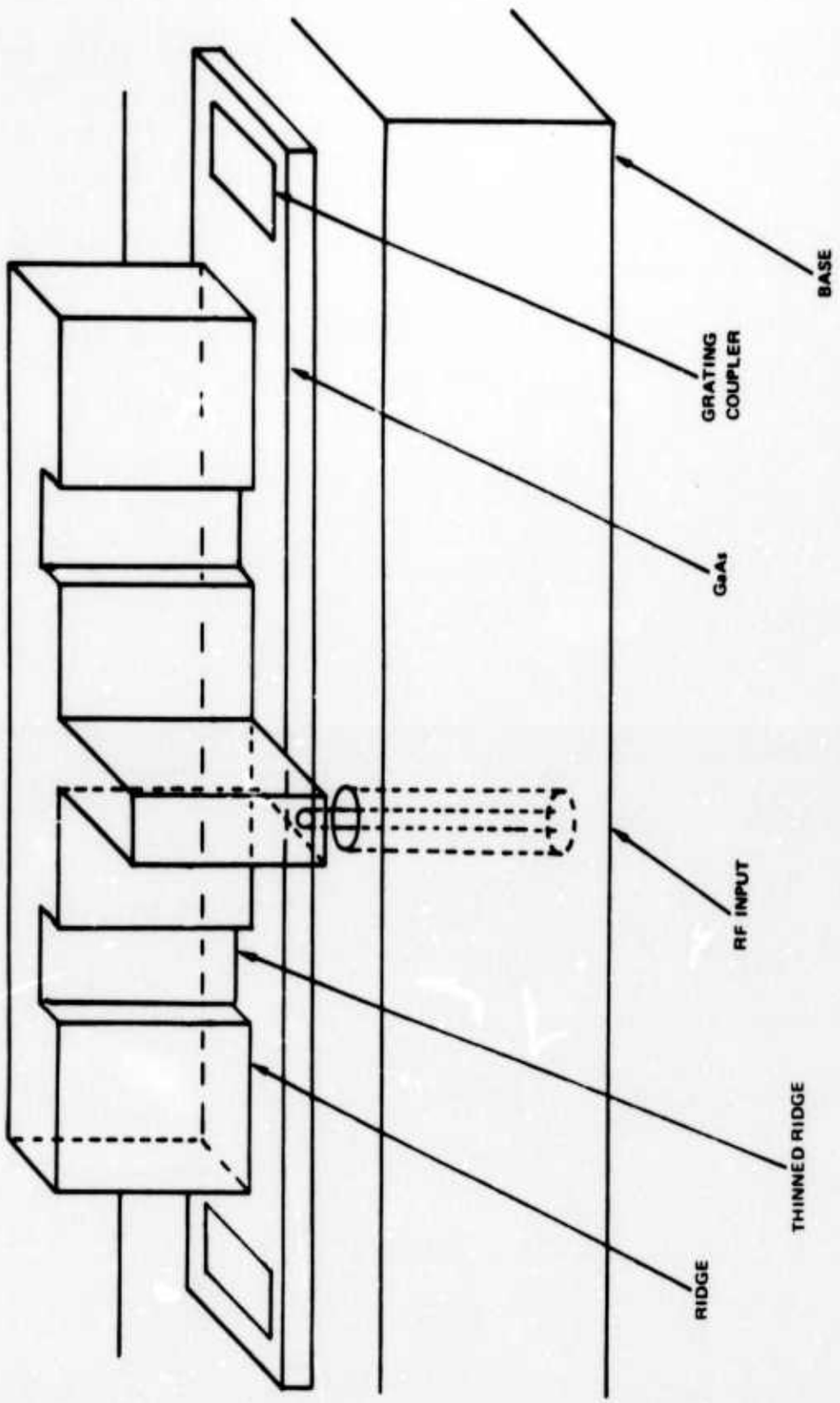

N03-241-2

FIG. 22

RESONANT RIDGE WAVEGUIDE MODULATOR

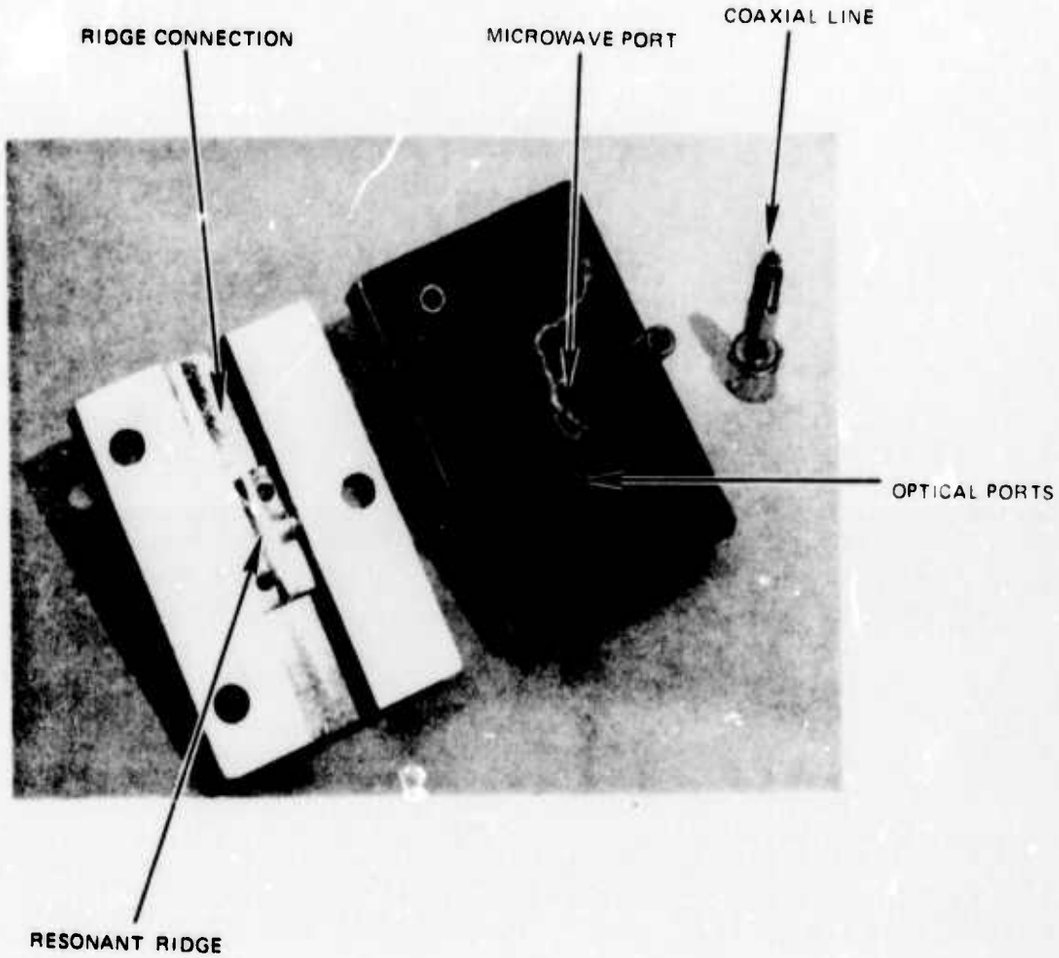

to those described in the previous report were carried out to determine the appropriate electrical parameters. Although the cross-sectional dimensions of the ridge gap itself were not changed, the remaining transverse dimensions of the structure were scaled down in order to prevent energy from leaking out of the open ends of the ridge structure. The measurements were not as accurate as the X-band measurements because the network analyzer calibration and components are poorer in the upper Ku-band frequency range.

In the Ku-band experiments, it was found that the effective index of refraction fell in the range of 2.8 to 3. The attenuation was found to be relatively constant at approximately 0.55 dB/cm and comparable to the X-band value of 0.5 dB/cm determined earlier. Though not accurately measured, there was a tendency for the index of refraction to increase with increasing frequency. Experiments were conducted with samples in the range of 25 to 40 microns thick. For reference purposes, a sketch of the ridge waveguide test section is reproduced in Figure 23. Data were obtained both with and without the terminated output coaxial line. This approach provided a set of self-consistent data from which the characteristic impedance, the velocity of propagation, and the losses would be estimated.

The impedance matching transformer will most likely be incorporated into a ridge section comprised of layers of air and GaAs. An analysis was made of the electrical properties of such a mini-ridge waveguide. The analysis was based on the ridge waveguide gap configuration shown in Figure 24 depicts the gap, the ground plane or base, the slab of GaAs (ε_1) and the remaining dielectric (ε_2). As an approximation, the microwave energy was considered to be uniformly distributed in the gap and the fringing fields were neglected. Transmission line theory relates the phase velocity to the inductance and capacitance per unit length; i.e., $v = 1/\sqrt{LC}$. From this relationship, it follows that the inductance per unit length is

$$L_o = \frac{1}{v_o^2 C_o} . \tag{32}$$

This inductance, to a first approximation, is independent of the dielectric medium filling the gap. The capacitance per unit length assuming static condition

$$\frac{1}{C} = \frac{h}{\varepsilon_1 W} + \frac{g}{\varepsilon_2 W} . \tag{33}$$

Equations 32 and 33 can be used to derive, then, an expression for the relative phase velocity of the composite medium in terms of the dielectric constant of the material and the thicknesses of the two layers. In particular,

$$\frac{v}{v_o} = \left(\frac{\varepsilon_o}{\varepsilon_1}\right)^{1/2} \left[\frac{1 + \frac{\varepsilon_1 h}{\varepsilon_2 h}}{1 + \frac{g}{h}}\right]^{1/2} \tag{34}$$

RIDGE WAVEGUIDE TEST SECTION

a) TEST SECTION

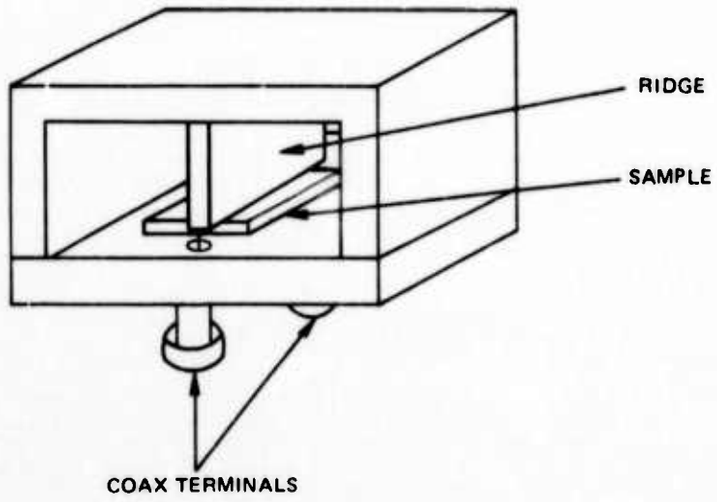

b) DETAILS OF RIDGE SECTION

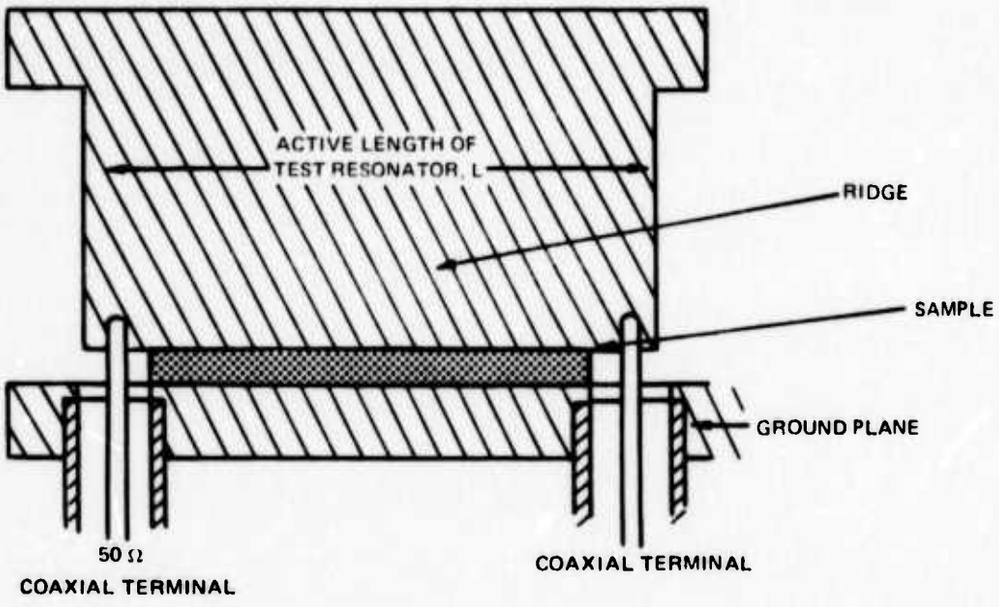

CROSS SECTION OF COMPOSITE MEDIUM UNDER RIDGE

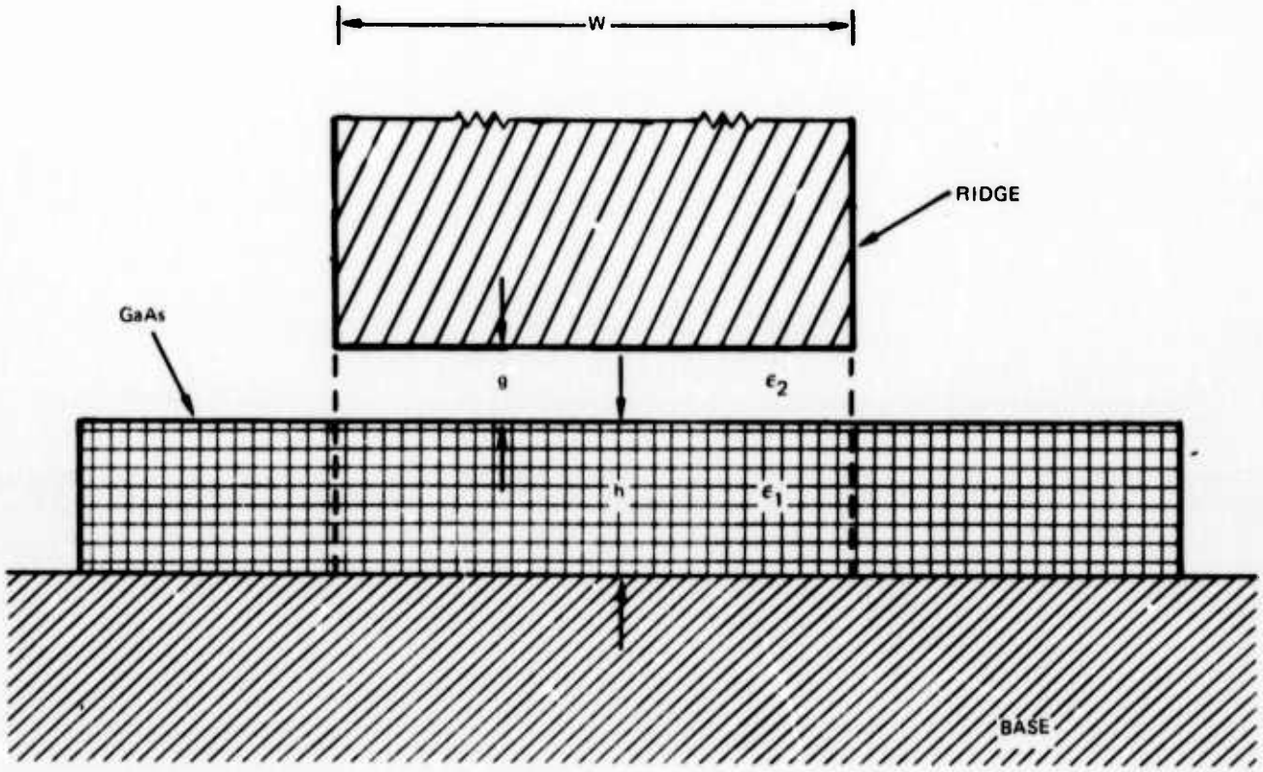

N03–241–3

An example for the impedance transformer that is relevant to our experiments is the case where h = 42 microns, g = 25 microns, $\varepsilon_2 = \varepsilon_o$ and the effective value of ε_1 is taken as 9. Using these values, the velocity of propagation is calculated to be 0.67 times that of an air-filled gap. If the ridge were completely surrounded with GaAs, the value would be 0.3. Since it is well-known that the ratio of characteristic impedances for a given geometry is proportional to the ratio of the velocities, the ratio derived above can be used for computing the characteristic impedance of a quarter wavelength section to be used for impedance transformation.

Another interesting example is to assume that the dielectric constant, ε_2, has a nominal value of 2 for a medium that is 2 microns thick. These parameters are appropriate to a thin dielectric layer that might be used for optical purposes on a 25-micron GaAs layer. The velocity ratio is found to be 0.35. This value indicates that the introduction of a small gap of dielectric material speeds up the propagating wave by 17 percent; therefore, larger periodic impedance steps would be required to compensate so as to make the velocity comparable to that of the optical wave in the GaAs.

The same approximations and analysis just discussed can be used to derive an expression for the power required to produce a given electric field in the GaAs portion of the composite medium. This field is the field responsible for the modulation of the ir beam. The dielectric layer deposited on the GaAs tends to increase the power required for a given value of electric field. With the passive dielectric layer, the incident power necessary to produce a given modulating field is

$$P = P_M \frac{\left(1 + \frac{\varepsilon_1 g}{\varepsilon_2 h}\right)^{3/2}}{\left(1 + \frac{g}{h}\right)^{1/2}} \qquad (35)$$

where P_M is the modulator power that would be required if the extra layer were absent. For the 2-micron passive layer considered above, the necessary microwave power is 67 percent higher than P_M.

Impedance matching experiments with a one-step impedance transformer to the GaAs filled mini-ridge waveguide were carried out with GaAs samples 42 microns thick. This thickness was used because thinner samples were unavailable at the time of the measurements. The characteristic impedance of the mini-ridge, GaAs-filled section was calculated to be about 8 ohms. From the well-known one-step impedance transformer relationship, $z = \sqrt{z_1 z_2}$, the quarter wave-step should, therefore, be a 20 ohm transmission line in order to properly match to a 50 ohm input terminal. It was determined experimentally that a 25-micron air layer gave good impedance matching. According to the sample calculations done earlier, the addition of a 25-micron air gap above the 42-micron GaAs layer gives a characteristic impedance transmission line of 27 ohms. The agreement between theory and experiment is, thus, good especially considering the approximate nature of the model and the tolerances on the structure dimensions. Also, for the composite section, the physical length

must take into account the ratio of velocities v/v_o which is calculated to be 0.67.

A sketch of the impedance matching transformer, which only includes the immediate region around a coaxial connection to the ridge section, is shown in Figure 25. The successful matching over a broad range of frequencies is illustrated in Figure 26 with Smith Chart plots of the reflection coefficient measured at one terminal of the ridge section while the other terminal was connected to a 50 ohm load. For both examples shown, the degree of impedance matching was such that, for $|\Gamma|^2 = < 0.04$ (i.e. VSWR < 1.5), a frequency range range of at least 1.5 GHz was available. Thus, the power in the modulator could vary by as much as 4 percent over a 1.5 GHz range of frequencies around an operating frequency near 16 GHz. The ridge dimensions were fine trimmed to the final step size in the ridge section until a match was obtained. These results are gratifying because step dimensions of approximately 25 microns are close to the working tolerances of machine shop practices. Similar results should be obtainable with the thinner samples as well as with dielectric coated samples. It should be noted that the useful bandwidth of the modulator will depend very strongly upon the range of amplitude variation that can be tolerated for a particular application.

The next step will be to fabricate a Ku-band traveling wave modulator section that can be used with optical excitation. In order to separate the microwave terminals from the optical terminals, the ridge, shown in Figure 27, has two 90° bends away from the optical path. The impedance matching transformers will actually be built into these sections. The matching transformers will be designed to compensate for the fact that the GaAs wafer extends only partially into these input and output lines to the ridge structure. The conditions for synchronization will be obtained by empirically determining the proper depth for the thinned sections of the ridge waveguide. As before these sections will be spaced a half-wavelength ($v_g/2f_\mu$) apart.

FIG. 25

IMPENDANCE MATCHING TRANSFORMER
50 OHM LINE TO RIDGE

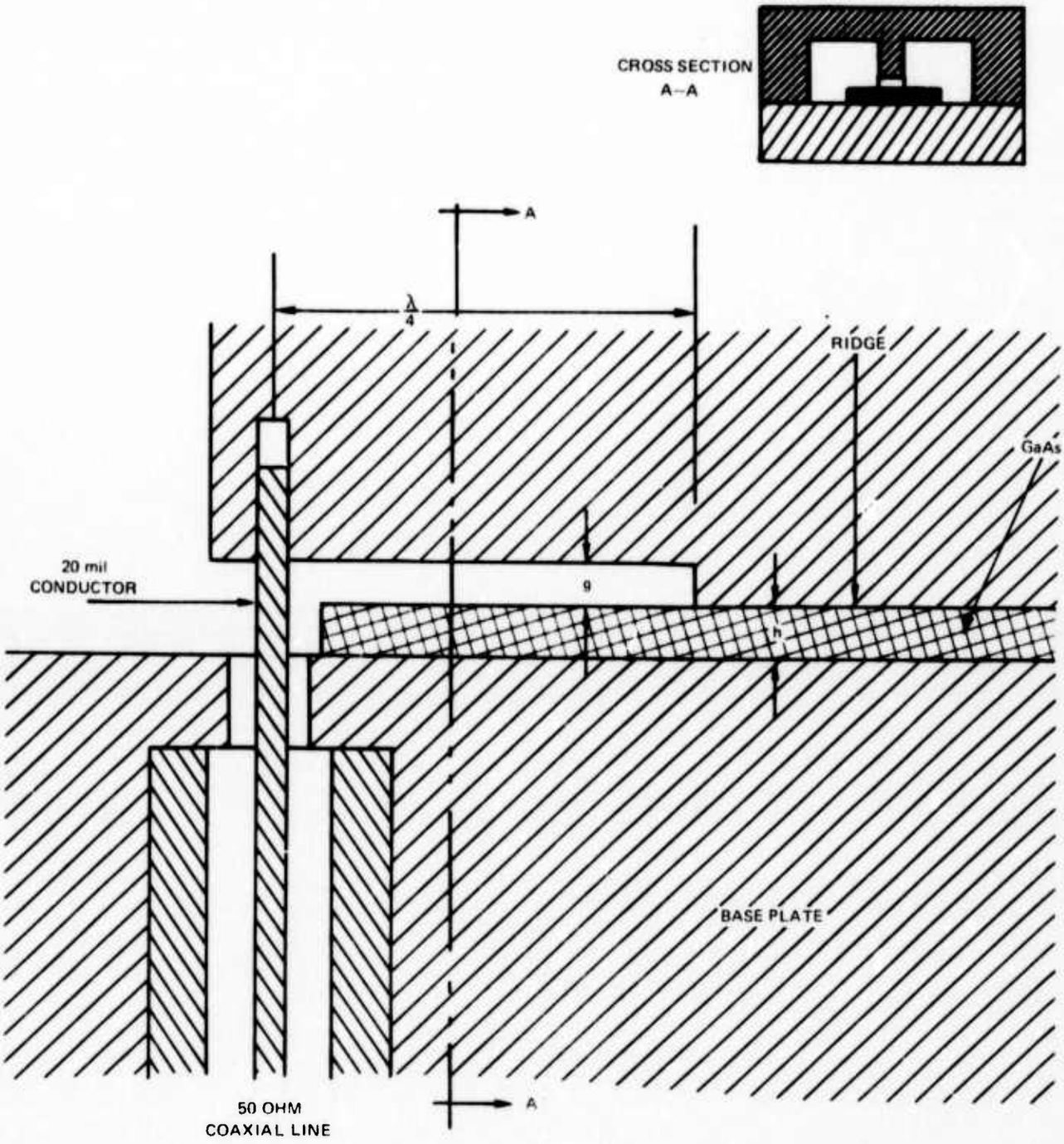

EXPERIMENTAL BROAD BAND MATCHING RESULTS

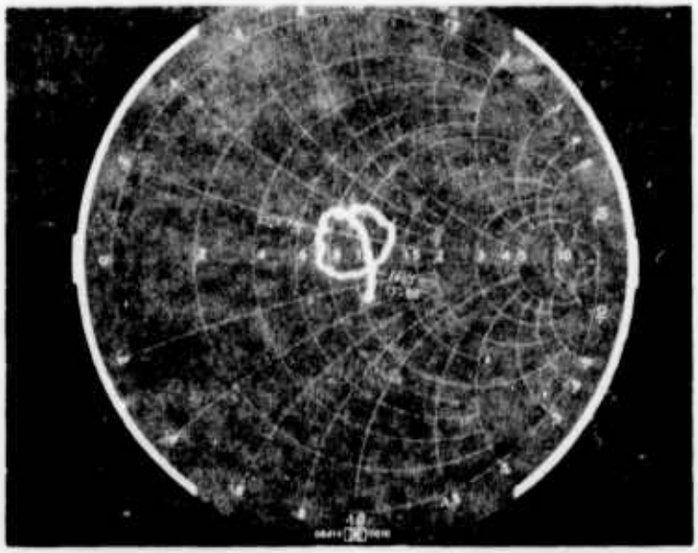

SAMPLE I 15–17 GHz (VSWR < 1.5)

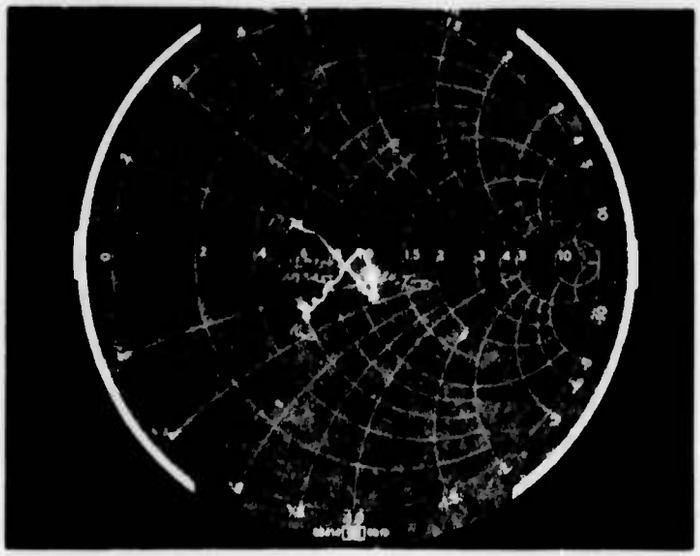

SAMPLE II 14 TO 15.5 GHz (VSWR < 1.5)

FIG. 27

SKETCH OF TRAVELING WAVE MODULATOR

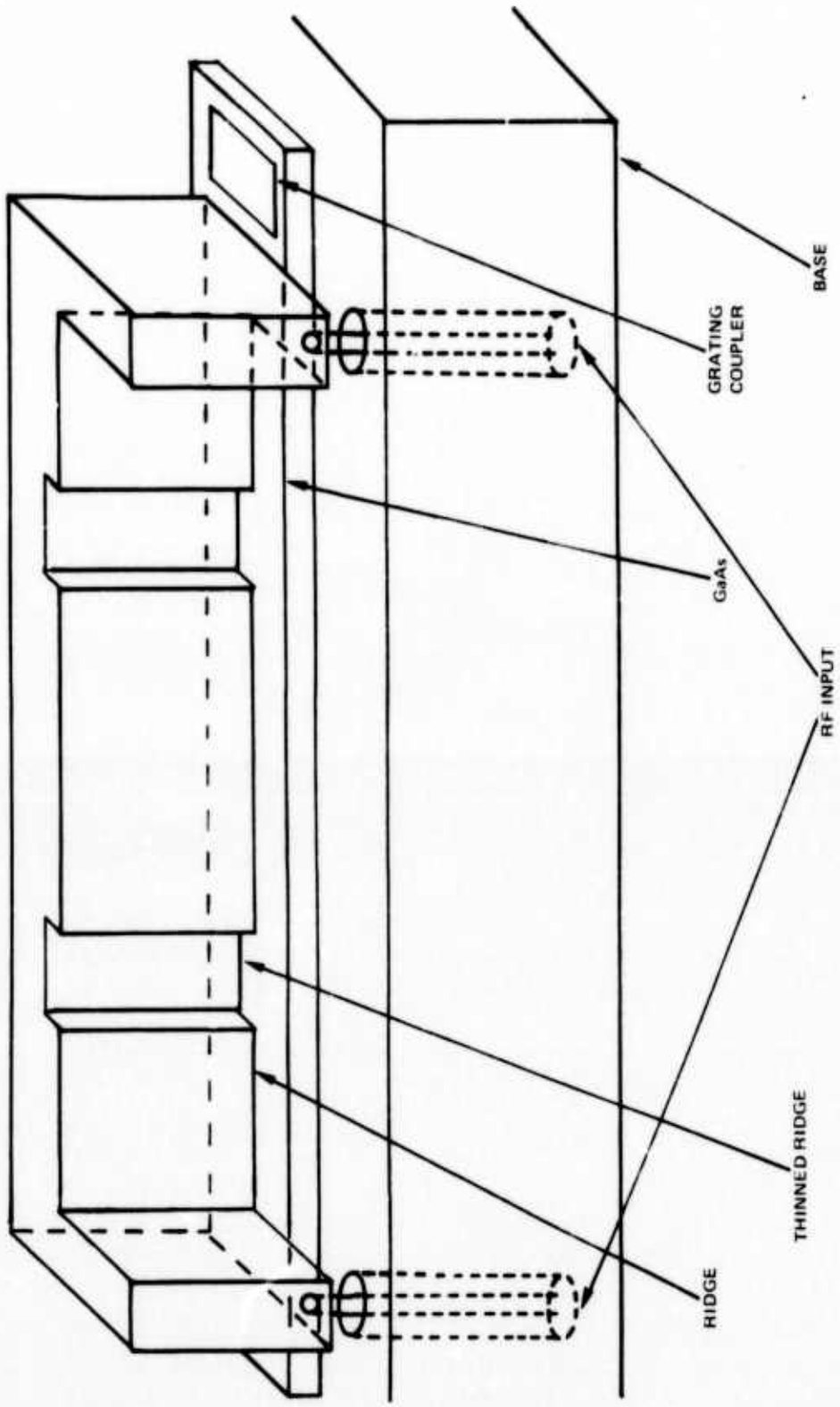

N03–241–1

6.0 Preliminary Work on Detection of Frequency-Chirped Modulation

The main purpose of the present program is to demonstrate a 500 MHz frequency-chirped modulation on a 10.6 micron laser beam. The system requirements to achieve this modulation are to phase modulate the laser and consequently to generate a side-band at 15.5 GHz offset from the carrier frequency. The chirp signal itself is imposed on the sideband signal, which in turn can be filtered out and used as the desired radar signal. The ultimate requirements on the linearity of the chirp and the stability of the sideband amplitude are very stringent. Meeting these stringent requirements will require sophisticated electronic regulations that are outside the scope of the present program. By using the thin-film microwave modulator developed under the present program, it should be possible to significantly reduce the burdens on the design of the electronic control circuitry for the microwave signal. This is primarily the result of a large reduction of the modulating power requirement for the thin-film element.

The modulation scheme, as described in previous section, is very straightforward technique for providing the microwave-chirped optical radar signal. A VCO, a voltage-controlled-oscillator, will be used to provide the microwave signal with the desired frequency modulation. Basically, the VCO will be a varactor tuned microwave oscillator with an output power of approximately 10 milliwatts in the 12-18 GHz range. Such voltage controlled oscillators are available with an input bandwidth of 10 MHz, sufficient for chirp signals of 3.3 microseconds duration. A microwave sweeper could easily provide the desired chirp but with a much longer pulse duration. The chirp microwave signal will then be amplified by a TWT amplifier up to about 16 watts. Because of the wideband characteristics of the TWT amplifier and the fact that only a small portion of the band is being used, namely 500 MHz, little distortion of the chirped signal is expected by the TWT amplifier.

To evaluate the chirped waveform, a heterodyne detection system, which consists of two frequency stable and line selecting CO_2 lasers, is required. Figure 28 shows some preliminary work done toward this experiment. The assembly of two lasers is nearly completed. A TEM_{oo} laser beam from one of these two stable lasers after being chopped is passed through the optical modulator. The chopper provides the basic repetition rate for the burst of pulses. Demonstration of chirp modulation on the laser beam will be accomplished in the balance of the experimental apparatus. A second very stable laser, using an isotope of CO_2 will produce a frequency offset from the first laser by 15.5 GHz. The two lasers will be directed towards the optical mixer to produce an rf signal which contains only the baseband chirp frequency spectrum. This baseband signal, in turn, can be converted into a frequency versus time presentation by applying the chirp signal to a broadband frequency discriminator and displaying the signal on an oscilloscope. A rough idea of the quality of the modulation can be obtained by comparing the output signal just described to a signal derived directly from the chirped VCO at 15.5 GHz.

FIG. 28

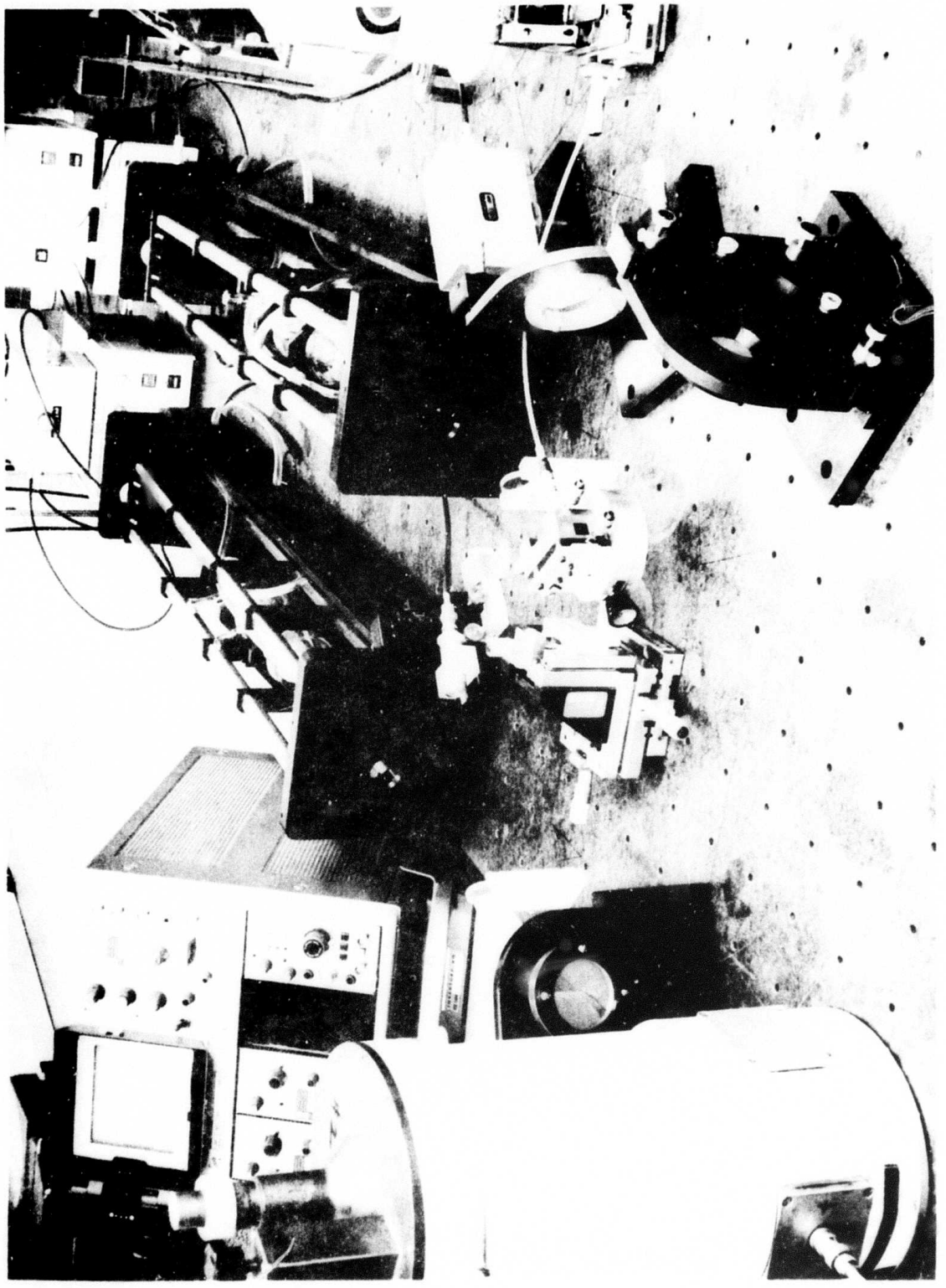

EXPERIMENTAL SETUP FOR HETERODYNE DETECTION SYSTEM

7.0 Future Plans

Future plans for the remaining period of the present program (from 25 March to 25 June, 1974), consists of three major tasks:

Task I: Design Analysis

The analysis of grating couplers will be extended to include a tailored groove depth in order to establish the conditions for maximizing α in a manner consistent with present microwave modulator design. A computer program will be constructed that will calculate $\alpha(x)$ and the near and far-field profiles of the coupled beam for an arbitrary variation of groove depth with x. The input coupling efficiency will then be calculated for an arbitrary input beam profile. On the basis of the theoretical result, optimum grating designs will be chosen for the thin-film modulator. Measurements of actual grating performance will be made and compared to theoretical predictions.

Task II: Fabrication of Broadband Microwave Modulator

The final design and fabrication of a broadband traveling wave thin-film modulator, matched to operate in the 16 GHz frequency range, will be made. Unless there are serious difficulties, the structure will be very similar to the one already described. In order to improve control over fabrication of the matching section, micro-electronic techniques will be considered for obtaining more accurate and reproducible impedance matching steps. This would include electroplating a thin section of the ridge directly onto the GaAs. The object will be to obtain a broadband structure with at least 500 MHz of useful bandwidth. From the results we have already obtained, the bandwidth may well exceed 1 GHz.

Task III: Demonstration of Frequency-Chirped Modulation

The main purpose of the present program is to demonstrate a 500 MHz frequency-chirped modulation on a 10.6 μm laser beam. An experimental arrangement involving a CO_2 laser transmitter, a frequency controlled microwave driver, a thin-film microwave modulator, a CO_2 laser local oscillator and a wideband infrared detector will be assembled. The general characteristics of the transmitter output waveforms will be investigated.

8.0 References

1. P. K. Cheo, Appl. Phys. Lett. 22, 241 (1973).

2. P. K. Cheo, Appl. Phys. Lett. 23, 439 (1973).

3. T. Y. Chang, N. Van Tran and C. K. N. Patel, Appl. Phys. Lett. 13, 357 (1968).

4. V. J. Corcoran, R. E. Cupp, J. J. Gallapher and W. T. Smith, Appl. Phys. Lett. 16, 316 (1970).

5. P. K. Cheo, J. M. Berak, W. Oshinsky and J. L. Swindal, Appl. Optics 12, 500 (1973).

6. K. Ogawa, W. S. C. Chang, B. L. Sopori and F. Rosenbaum, IEEE J. Quant. Electron. QE-9, 29 (1973).

7. P. K. Cheo and M. Gilden, to be presented at Int. Quant. Electron. Conference, June 10-13, 1974, in San Francisco, California.

8. P. K. Cheo, M. Gilden, J. F. Black and J. L. Swindal, UARL Semi-Annual Tech. Report M921513-4, September 1973, Contract No. N00014-73-C-0087.

9. P. K. Tien, R. Ulrich, and R. J. Martin, Appl. Phys. Lett. 14, 291 (1969).

10. A. Yariv, IEEE J. Quant. Elect. QE-9, 919 (1973).

11. S. T. Peng, T. Tamir and H. L. Bertoni, Digest of 2nd Top. Meet. on Int. Opt., Jan. 21-24, 1974, Paper TuB8.

12. T. Tamir, Antenna Theory, Part 2 (P. E. Collin and F. J. Zucker, ed), McGraw Hill Book Company, New York (1969).

13. T. Tamir, Optik 38, 270 (1973).

14. T. Tamir and H. L. Bertoni, Topical Meeting on Integrated Optics, Las Vegas, Feb. 7-10, 1972, Paper MB3.

15. T. Tamir and A. A. Oliner, Proc. IEE 110, 310 (1963).

16. P. K. Tien, Appl. Optic 10, 2395 (1971).

17. D. Marcuse, Bell Syst. Tech. J. 48, 3187 (1969).

18. These computations were made in collaboration with K. Ogawa by using the existing computer program at Washington University in St. Louis.

19. T. Tamir, Polytechnic Institute of New York (to be published).

20. J. W. Goodman, Introduction to Fourier Optics (McGraw Hill, New York 1968), 69.